Received: 17 November 2019 | Revised: 2 April 2020 | Accepted: 25 April 2020

DOI: 10.1111/gcb.15170

Check for updates

PRIMARY RESEARCH ARTICLE

Global Change Biology WILEY

Continental-scale tree-ring-based projection of Douglas-fir growth: Testing the limits of space-for-time substitution

Stefan Klesse[1,2] | Robert Justin DeRose[3,4] | Flurin Babst[1,2,5] | Bryan A. Black[1] | Leander D. L. Anderegg[6,7] | Jodi Axelson[8] | Ailene Ettinger[9] | Hardy Griesbauer[10] | Christopher H. Guiterman[1] | Grant Harley[11] | Jill E. Harvey[12] | Yueh-Hsin Lo[13] | Ann M. Lynch[1,14] | Christopher O'Connor[15] | Christina Restaino[16] | Dave Sauchyn[17] | John D. Shaw[3] | Dan J. Smith[18] | Lisa Wood[19] | Jose Villanueva-Díaz[20] | Margaret E. K. Evans[1]

[1]Laboratory of Tree-Ring Research, University of Arizona, Tucson, AZ, USA

[2]Swiss Federal Research Institute WSL, Swiss Forest Protection, Birmensdorf, Switzerland

[3]U.S. Forest Service, Rocky Mountain Research Station, Forest Inventory and Analysis, Ogden, UT, USA

[4]Department Wildland Resources and Ecology Center, Utah State University, Logan, UT, USA

[5]Department of Ecology, W. Szafer Institute of Botany, Polish Academy of Sciences, Krakow, Poland

[6]Department of Integrative Biology, University of California, Berkeley, CA, USA

[7]Department of Global Ecology, Carnegie Institution for Science, Stanford, CA, USA

[8]Department of Environmental Science, Policy, and Management, University of California, Berkeley, CA, USA

[9]The Nature Conservancy, Seattle, WA, USA

[10]Ministry of Forests, Lands, Natural Resource Operations and Rural Development, Prince George, BC, Canada

[11]Department of Geography, University of Idaho, Moscow, ID, USA

[12]Natural Resources Canada, Canadian Forest Service, Edmonton, AB, Canada

[13]Department of Science, Universidad Publica de Navarra, Pamplona, Spain

[14]U.S. Forest Service, Rocky Mountain Research Station, Tucson, AZ, USA

[15]U.S. Forest Service, Rocky Mountain Research Station, Missoula, MT, USA

[16]University of Nevada Cooperative Extension, Reno, NV, USA

[17]Prairie Adaptation Research Collaborative, University of Regina, Regina, SK, Canada

[18]Department of Geography, University of Victoria, Victoria, BC, Canada

[19]Ecosystem Science and Management, University of Northern British Columbia, Prince George, BC, Canada

[20]Instituto Nacional de Investigaciones Forestales y Agropecuarias, CENID-RASPA, Gomez Palacio, Mexico

Correspondence
Stefan Klesse, Swiss Federal Research Institute WSL, Swiss Forest Protection, Birmensdorf, Switzerland.
Email: stefan.klesse@wsl.ch

Funding information
Fundacja na rzecz Nauki Polskiej, Grant/Award Number: POIR.04.04.00-00-5F85/18-00; National Science Foundation, Grant/Award Number: DBI-0735191, DBI-1265383 and DBI-1802893; National Institute of Food and Agriculture, Grant/Award Number: 2016-67003-24944; European Regional Development Fund

Abstract

A central challenge in global change research is the projection of the future behavior of a system based upon past observations. Tree-ring data have been used increasingly over the last decade to project tree growth and forest ecosystem vulnerability under future climate conditions. But how can the response of tree growth to past climate variation predict the future, when the future does not look like the past? Space-for-time substitution (SFTS) is one way to overcome the problem of extrapolation: the response at a given location in a warmer future is assumed to follow the response at a warmer location today. Here we evaluated an SFTS approach to projecting future growth of Douglas-fir (*Pseudotsuga menziesii*), a species that occupies an exceptionally large environmental

 © 2020 John Wiley & Sons Ltd

space in North America. We fit a hierarchical mixed-effects model to capture ring-width variability in response to spatial and temporal variation in climate. We found opposing gradients for productivity and climate sensitivity with highest growth rates and weakest response to interannual climate variation in the mesic coastal part of Douglas-fir's range; narrower rings and stronger climate sensitivity occurred across the semi-arid interior. Ring-width response to spatial versus temporal temperature variation was opposite in sign, suggesting that spatial variation in productivity, caused by local adaptation and other slow processes, cannot be used to anticipate changes in productivity caused by rapid climate change. We thus substituted only climate sensitivities when projecting future tree growth. Growth declines were projected across much of Douglas-fir's distribution, with largest relative decreases in the semiarid U.S. Interior West and smallest in the mesic Pacific Northwest. We further highlight the strengths of mixed-effects modeling for reviving a conceptual cornerstone of dendroecology, Cook's 1987 aggregate growth model, and the great potential to use tree-ring networks and results as a calibration target for next-generation vegetation models.

KEYWORDS

carbon sequestration, climate sensitivity, Douglas-fir, forest inventory, growth projection, mixed-effects model, tree growth, tree ring

1 | INTRODUCTION

A central challenge in global change research is projecting organism or ecosystem responses to future conditions—for example, warmer temperatures and increased evaporative water demand. Forests cover about 30% of the Earth's land surface and sequester vast amounts of carbon from the atmosphere, part of which is fixed in woody biomass for decades to centuries (Pan et al., 2011). For this reason, the impact of changing climate on forest ecosystems is expected to directly and/or indirectly feedback on the climate (Bonan, 2008). In the fifth realization of the Coupled Model Intercomparison Project (CMIP5), significant uncertainty is associated with the future behavior of the terrestrial carbon sink (Friedlingstein et al., 2014). While model ensembles generally project the terrestrial carbon sink to increase, the spread among individual models is remarkable (Schurgers, Ahlström, Arneth, Pugh, & Smith, 2018). Reducing uncertainties regarding forest ecosystem behavior under future temperature and precipitation regimes requires observations with a large spatiotemporal scope. However, current large-scale observation networks lack temporal resolution (national forest inventories), have limited temporal depth (eddy-covariance flux towers), or yield only indirect measures of tree growth (remotely sensed metrics of greenness). Tree rings complement these other data streams by offering annually resolved data of radial tree growth on much longer time scales (Babst et al., 2018; Klesse, Babst, et al., 2018). Indeed, tree-ring records have historically been used to put current climate conditions and trajectories in the context of climate variability over centuries to millennia (e.g., Cook et al., 2015; Wilson et al., 2016). These climate reconstructions rely upon the principle of uniformitarianism, that is, that the growth response to a limiting factor was the same in the recent past (instrumental period) as in the deep past (pre-instrumental period; Fritts, 1976). That is, the statistical relationship between ring-width variation and the target climate variable is assumed to be stable over time. In the Anthropocene, an era of unprecedentedly rapid change of the Earth's climate system, this assumption is increasingly violated (Babst et al., 2019; Gustafson, 2013; Wilmking et al., 2020), and is even more likely to be violated in the future as the nonlinear increase in atmospheric evaporative demand with rising temperatures aggravates drought stress on trees. The extrapolation of past climate–growth relationships into conditions outside the domain of calibration may yield erroneous projections (Fritts, 1976). Indeed, Charney et al. (2016) found that a shift from positive to negative temperature sensitivity of boreal forests during the 21st century is expected to offset projected growth increase under the assumption of uniformitarianism. More recently, Babst et al. (2019) found global evidence of just such a shift, from temperature-limited forest growth toward increased limitation by atmospheric water demand, during the late 20th century.

One potential solution to the problem of extrapolation is the use of space-for-time substitution (SFTS; Pickett, 1989). Under SFTS, it is presumed that the growth of trees at relatively warmer sites today can tell us how trees at relatively cooler sites may grow in a warmer future. Indeed, ecological niche theory suggests that organismal performance (e.g., growth) should vary in a predictable fashion, decreasing continuously from the niche optimum to its edge (Hutchinson, 1978; Maguire, 1973). In a now classic figure in dendrochronology, Fritts, Smith, Cardis, and Budelsky (1965, their figure 2) went one step further in describing predictable variation in tree-ring widths: average ring width and ring-width sensitivity

to interannual climate variation trend in opposite directions across the environmental gradient from the forest interior to the forest edge (see also Anderegg & HilleRisLambers, 2019; Knapp, Ciais, & Smith, 2017), a prediction that we illustrate in Figure 1. An important caveat, however, is that SFTS relies on the assumption that the process(es) giving rise to spatial variation are the same as those giving rise to temporal variation. Furthermore, for spatial variation in an ecological variable to accurately predict the response to temporal environmental change, the time scale of a given environmental change versus that of the driving ecological process must be comparable (Damgaard, 2019). A vast spatial network of time-series data makes it possible to evaluate these assumptions underlying SFTS.

To capture spatial and temporal variation in tree growth, we advocate for the return to one of the conceptual cornerstones of dendrochronology: the aggregate tree growth model (Cook, 1987), in which absolute ring widths are predicted as a function of four simultaneous influences: tree size, climate, "endogenous disturbances" (i.e., competitive pressure from neighbors), and exogenous disturbances (e.g., insect outbreaks). Here, we apply the aggregate growth model within a generalized mixed-effects framework to quantify absolute growth in bole diameter (a metric related to carbon sequestration) as a function of simultaneous variation in climate and tree size. Mixed-effects models are commonly used in (dendro-) ecology, but their application to variation in absolute ring-width time series, that is, without prior "detrending," is less common (but see e.g., Canham, Murphy, Riemann, McCullough, & Burrill, 2018; González de Andrés et al., 2017; Martin-Benito, Kint, del Río, Muys, & Cañellas, 2011; Martínez-Vilalta, López, Loepfe, & Lloret, 2012; Morrongiello & Thresher, 2015; Redmond, Kelsey, Urza, & Barger, 2017). We constructed a model that explicitly quantifies ring-width variation in response to spatial versus temporal climate variation by specifying two kinds of climate influences on tree growth: (a) climate normals that vary across space, which influence overall productivity (the average ring width at a given site) and (b) climate that varies over time at a given location, which drives interannual ring-width variability.

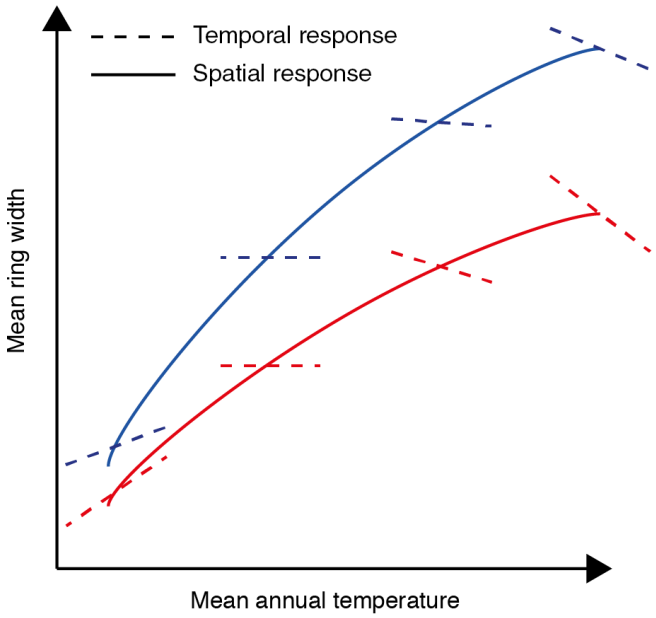

FIGURE 1 Predicted variation in average ring width (i.e., productivity, solid lines) and climate sensitivity (dashed lines) across a gradient of mean annual temperature (MAT) for two levels of precipitation (line colors). Across space, average ring width is expected to increase with increasing MAT, with higher productivity under wet conditions (blue) compared to dry (red) conditions. Under cold conditions (low MAT), interannual variation in temperature (dashed lines) may have a positive effect on growth versus a negative effect in the rest of the distribution. The impact of interannual climate variation (the slope of dashed lines) is predicted to be weaker under mesic conditions than dry conditions

We used Douglas-fir (*Pseudotsuga menziesii* [Mirb.] Franco) as a particularly compelling species for developing a mixed-effects modeling framework to quantify spatial and temporal variation in growth and project future tree growth. It is the most abundant and economically important tree species in North America, with a distribution ranging from 17°N to 55°N. Corresponding to its vast geographic range, Douglas-fir grows under climate conditions with mean annual temperatures (MATs) between −0.5 and 19.5°C and cumulative annual precipitation from 300 to 4,800 mm. Furthermore, it is widely planted outside of its native range (Isaac-Renton, Roberts, Hamann, & Spiecker, 2014). We use the mixed-effects model to address two research questions across its native range: First, do productivity and climate sensitivities vary across environmental gradients in a predictable pattern, as described by Fritts et al. (1965) and delineated in Figure 1? Second, are spatial and temporal variability in ring widths substitutable so that spatial variability may be used to anticipate the response of Douglas-fir to climate change of the near future?

We used modeled climate sensitivities and the output of 16 general circulation models to project growth changes for the 2011–2040 period under contrasting assumptions: (a) climate sensitivity at a given location does not change over time with changing climate normals (uniformitarianism) versus (b) climate sensitivity at a given location is modified by changing climate normals, that is, relying on SFTS of climate sensitivities.

2 | MATERIALS AND METHODS

2.1 | Study area and tree-ring data

Douglas-fir comprises two varieties: the coastal variety ssp. *menziesii*, which occurs from California to British Columbia along the Pacific coast and coastal mountain ranges east to the crest of the Sierra Nevada and Cascade ranges; and the interior variety ssp. *glauca*, which is found throughout the intermountain west and North American cordillera from British Columbia and Alberta to southern Mexico (Figure 2).

We compiled a tree-ring data network consisting of 30,388 tree-ring time series from 2,699 sites, totaling 2,706,098 growth rings over the 1902–2016 period of analysis. The data at 319 of these sites were downloaded from the International Tree Ring Data Bank (ITRDB; https://www.ncdc.noaa.gov/paleo-search/?dataTypeId=18, January 2017),

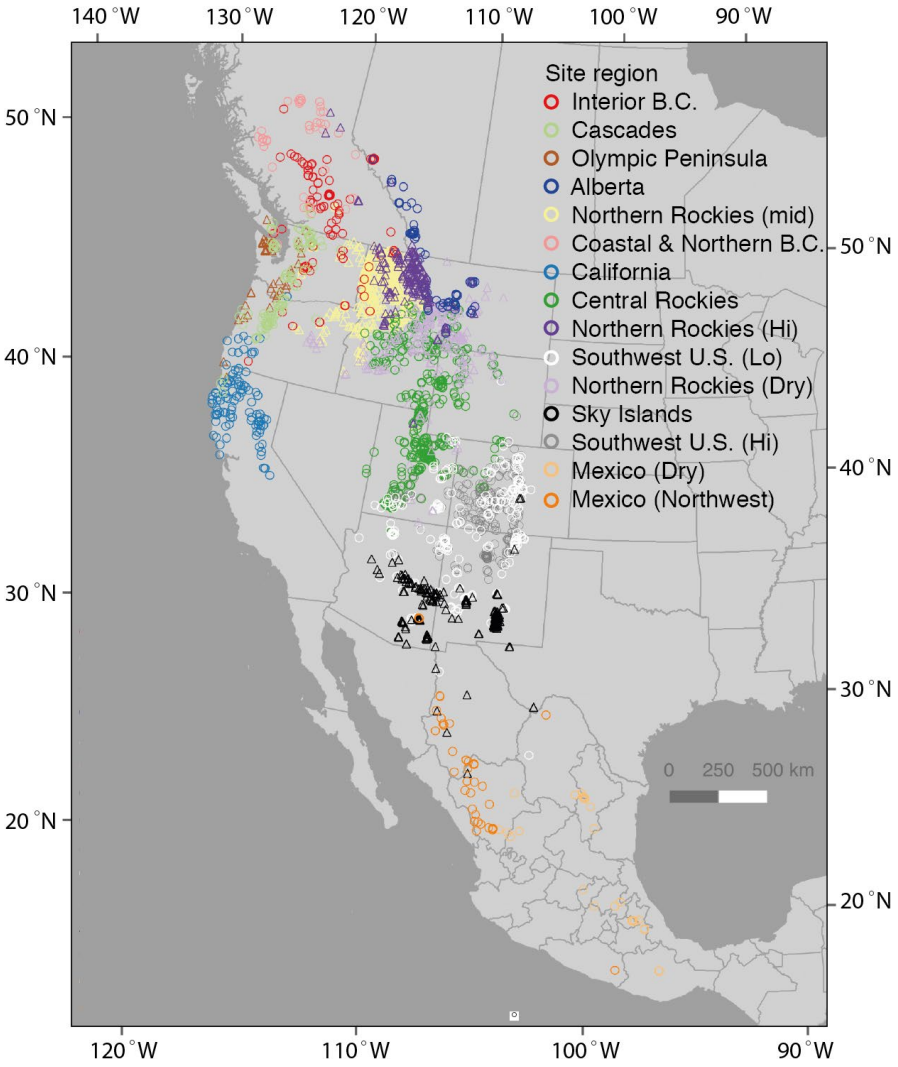

FIGURE 2 Distribution of Douglas-fir tree-ring sampling sites across western North America. Colors represent the 15 climatic-geographic regions defined via supervised self-organized mapping described in Section 2

whereas the data of an additional 630 sites were directly contributed by the tree-ring community and co-authors. Similar to the ITRDB, the sampling schemes underlying this second collection ranged from elevation gradient (Anderegg & HilleRisLambers, 2019; Case & Peterson, 2005; Guiterman, 2016; Littell, Peterson, & Tjoelker, 2008; Restaino, Peterson, & Littell, 2016) and gridded designs (O'Connor, Falk, Lynch, & Swetnam, 2014) to targeted sampling for dendroclimatological or -entomological reconstructions (e.g., Allen et al., 2013; Martin et al., 2019; Razavi, Elshorbagy, Wheater, & Sauchyn, 2015; Ryerson, Swetnam, & Lynch, 2003; Swetnam & Lynch, 1989). We also included 2,617 tree-ring time series from 1,750 permanent forest inventory plots of the U.S. Forest Service Interior West-Forest Inventory and Analysis (FIA) program, which is presently the most extensive systematically sampled tree-ring collection in the region (DeRose, Shaw, & Long, 2017). The FIA plot network was designed to representatively sample all forested lands of the U.S. with one plot per 2,428 ha (Bechtold & Patterson, 2005); hence, tree-ring sampling in this plot network results in a dataset, that is, to a large degree, spatially and ecologically unbiased. The number of increment cores per site (sample replication) ranged from 1 to 225 time series across this network, with an average of 1.5 samples at FIA sites versus 29 at non-FIA sites. Thus, the majority of sampling locations came from the FIA collection (65%), whereas the majority of the tree-ring time series came from the ITRDB or contributed collections (91%).

2.2 | Climate data

Climate data were extracted for each of the 2,699 sites using ClimateNA v5.50 (Wang, Hamann, Spittlehouse, & Carroll, 2016; http://tinyurl.com/ClimateNA), which is based on the CRU TS3.24 gridded historical monthly data product spanning the years 1901–2016. ClimateNA downscales and interpolates the CRU data to adjust the mean and variance of climate time series to elevation- and location-specific values (Wang et al., 2016).

Future climate projections were taken from 16 Atmosphere-Ocean General Circulation Models (AOGCMs) of the CMIP5 multi-model dataset, that is, the IPCC Assessment Report 5 (2013), also extracted from ClimateNA for each site. We focused on climate normal projections for the 2011–2040 period under the business-as-usual emission scenario RCP8.5, which projects the consequences

of an extra 8.5 W/m^2 of energy retained by the atmosphere in 2100 compared to the pre-industrial baseline. The projected increase in winter temperature ranges from around +1°C in Mexico and the U.S. Southwest to +2.5–3°C in the Pacific Northwest and Canada compared to the 1910–2010 long-term average.

2.3 | Generalized linear mixed-effects model

Because growth rings within a time series and time series within a sampling location are not independent, we modeled tree-ring-width variation using a generalized mixed-effects model. This framework allowed us to simultaneously estimate the (fixed) effects of tree size, climate normals, and time-varying climate on the width of annual growth rings, as well as account for unexplained variation between samples and locations (via random intercept and random slope terms). We first describe a baseline model, followed by a series of model variants. The baseline model has the form:

$$\begin{aligned} RW_{p,s,t} \sim{}& \beta_0 + \beta_1 TS_{p,s,t-1} + \boldsymbol{\beta_{2i}} \boldsymbol{CNC}_{i,p} + \boldsymbol{\beta_{3j,k}} \boldsymbol{CA}_{j,k,p,t} \\ &+ \boldsymbol{\beta_{4i}} \boldsymbol{CNC}_{i,p} * TS_{p,s,t-1} + \boldsymbol{\beta_{5i,j,k}} \boldsymbol{CNW}_{i,p,t} * \boldsymbol{CA}_{j,k,p,t} \\ &+ \beta_6 CNC_{1,p} * CNC_{2,p} + \boldsymbol{\beta_{7j,k}} CNW_{1,p,t} * CNW_{2,p,t} * \boldsymbol{CA}_{j,k,p,t} \\ &+ \beta_8 CNC_{1,p} * CNC_{2,p} * TS_{p,s,t-1} + \gamma_{0p,s} + \gamma_{1p,s} TS_{p,s,t-1} + \gamma_{2p,s} PA_{p,s,t} \\ &+ \varepsilon_{p,s,t}, \end{aligned} \tag{1}$$

where ring width *RW* of sample *s* in year *t* is nested in plot *p*. $RW_{p,s,t}$ is influenced by tree size $TS_{p,s}$ of the preceding year *t* − 1, climate normals $\boldsymbol{CNC}_{i,p}$ (climate normals that are constant and hence do not include the time index *t*) and $\boldsymbol{CNW}_{t,i,p}$ (30-year moving window climate normals), annually varying seasonal climate variables $\boldsymbol{CA}_{j,k,p,t}$ (specific to each year *t*), and random effects γ_0, γ_1, and γ_2 specific to each sample *s* nested within each sampling location *p*. *TS* is the age-specific cumulative radius of each sample

$$\text{Projection uncertainty} = \sqrt{\text{FEU}^2 + \text{SDP}^2}. \tag{2}$$

summing from the first radial increment, assuming that the first measured growth ring originates at the pith ($TS_{a=0}$ = 0). This fixed effect (*TS*) serves the same purpose as the dendrochronological practice of detrending—that is, it accounts for the decline in absolute ring width associated with increasing tree bole diameter. The index *i* varies from one to two, specifying MAT and mean annual precipitation (MAP). The index *j* specifies two climate variables—mean maximum temperature and cumulative precipitation—and the index *k* specifies eight 2-month seasons, beginning with the previous year's June and July, August and September, October and November, …, through the current year's September and October (noting that the winter period previous December to current year February is 3-month season). The scalars β_0, β_1, β_6, and β_8 and the vectors $\boldsymbol{\beta_{2\text{–}5,7}}$, along with the random effects γ_0, γ_1, and γ_2 are regression parameters estimated by the model.

The influence of tree size *TS* and constant climate normals $\boldsymbol{CNC}_i$ on *RW* were fit using natural cubic splines with a B-spline basis and 3 *df*, with knots placed at the 33rd and 67th quantiles of each variable (Boor, 1978). We included only linear terms for the time-varying seasonal climate variables $\boldsymbol{CA}_{j,k}$ to limit model complexity; these terms ($\boldsymbol{\beta_3}$) capture the plastic response of tree growth to local interannual climate variation. To capture variability across environmental gradients in size-related trends of radial increments, we specified interactions between *TS* and each of the two $\boldsymbol{CNC}_i$ variables ($\boldsymbol{\beta_4}$ and $\boldsymbol{\beta_8}$). Expecting climate sensitivity to vary across populations growing under different climatic conditions (Fritts et al., 1965), we also included (two- and three-way) interactions between $\boldsymbol{CNW}_i$ and $\boldsymbol{CA}_{j,k}$ variables ($\boldsymbol{\beta_5}$ and $\boldsymbol{\beta_7}$). These interaction terms (particularly between $\boldsymbol{CNW}_i$ and $\boldsymbol{CA}_{j,k}$) are critical to the space-for-time approach in that they capture spatial variation in climate sensitivities driven by variation in MAT and MAP. Note the time index ***t*** included on the climate normals in the interaction term ($\boldsymbol{\beta_{5i,j,k}} \boldsymbol{CNW}_{i,p,t} * \boldsymbol{CA}_{j,k,p,t}$). These climate normals were calculated along a moving 30-year average to better capture the influence of decade-scale climate variability on interannual variability in growth increments. Hence, we modeled overall productivity as a function of a constant 110-year climate normal ($\boldsymbol{\beta_{2i}} \boldsymbol{CNC}_{i,p}$ and $\boldsymbol{\beta_6}$ $CNC_{1,p} * CNC_{2,p}$), whereas we modeled spatial variability in climate sensitivities as a function of time-varying 30-year climate normals ($\boldsymbol{CNW}_i$). Because of missing climate data before 1902, growth rings associated with the first 30 years have the same climate normal. After 1932, the climate normal was calculated over the 1903–1932 period, and so on. Last, we also included an interaction between the two climate normals ($\boldsymbol{CNC}_i$). Four fixed effects in the model, the $\boldsymbol{\beta_2}$, $\boldsymbol{\beta_4}$, β_6 and β_8 terms, reflect only spatial variation in the width of growth rings.

Three kinds of random effects, $\gamma_{0p,s}$, $\gamma_{1p,s} TS_{p,s,t-1}$, and $\gamma_{2p,s} PA_{p,s,t}$, were included for each sample nested within a sampling location. The first is an intercept modification, $\gamma_{0p,s}$, capturing variation in the average ring width among sites and samples within sites, caused by unquantified factors such as stand density, soil, or micro-site conditions. The second term, $\gamma_{1p,s} TS_{p,s,t-1}$, is a random modification of the effect of tree size, capturing the degree to which the shape of the size-related trend in absolute ring widths is influenced by (unquantified) tree- and site-specific factors, adding further flexibility to this detrending analogue. These two terms, the random intercept modification and random modification of the influence of tree size, have the added benefit that they adjust for error associated with the assumption that the first ring of each time series starts at pith. The third random effect, $\gamma_{2p,s} PA_{p,s,t}$, was motivated by previous work demonstrating that the ITRDB versus FIA collections differ systematically in climate sensitivities (Klesse, DeRose, et al., 2018). This term captures variation in the sensitivity to cumulative precipitation anomalies across the water year (previous year June to current year October) among sites and samples within sites that are attributable to micro-site conditions such as slope, aspect, and soil quality.

We chose a Gamma error distribution because ring-width variability is proportional to the mean ring width, giving rise to heteroscedasticity in the data. A gamma response requires a log-link, thus all ring-width values were transposed by +0.01 mm to accommodate non-positive (zero) values—that is, missing rings. We weighted each

plot in proportion to its median distance to all other sites to account for over- (under-) representation of heavily (sparsely) sampled regions of Douglas-fir's geographic distribution. This baseline model was implemented using the *lme4* package (Bates, Mächler, Bolker, & Walker, 2015) in R version 3.5.1 (R Core Team, 2018) in the XSEDE and CyVerse environment (Merchant et al., 2016; Stewart et al., 2015; Towns et al., 2014). An R script implementing the model is provided in the Supplementary Material.

Different parts of the dataset were collected for different purposes. Whereas the FIA dataset was designed to be spatially and ecologically unbiased, most of the ITRDB data in the Western US were collected to maximize climate signal (for reconstructing climate), by sampling trees growing under marginal conditions where the sensitivity of tree growth to climate variation is strongest (Klesse, DeRose, et al., 2018). To investigate the effect of using these different datasets as well as address contrasting patterns of sample replication per site (i.e., at FIA versus other sites), we applied the baseline model described above in three ways:

1. Using only tree-ring time series from the FIA network, hereafter referred to as the "FIA model";
2. Using all data ("ALL model");
3. Using all data, but weighting sites inversely proportional to their sample replication by dividing the distance weight by the number of samples per site and year. This has the effect of downweighting heavily replicated sites and years so that each site ultimately has equal weight ("ALL-W model").

Early tests indicated better model performance (calibration-verification statistics) when the two varieties of Douglas-fir were modeled separately. Therefore, we present only results based on separate models for the coastal versus interior varieties.

2.4 | Model calibration and verification

We evaluated model performance (fit to data) in terms of two important components of tree growth—productivity and climate sensitivity. With respect to productivity, we compared model-predicted average ring width against independently collected productivity estimates derived from the U.S. Forest Service FIA Program: site index at base age 50, that is, the average height of dominant and codominant trees in a fully stocked, even-aged stand (Bechtold & Patterson, 2005). That is, we evaluated the ability of models to reproduce spatial variation in productivity across the U.S. portion of Douglas-fir's geographic distribution.

The ability of models to reproduce temporal (interannual) variability was assessed by calculating Pearson correlation coefficients between observed versus predicted ring-width time series at three scales: the sample, site, and region. At the scale of a sample (increment core), we detrended both the observed ring-width time series and the ring-width time series predicted by the above statistical models, including all fixed and random effects, using a cubic smoothing spline with a 50% frequency cutoff at 30 years. By detrending both observed and predicted time series, we focused on the ability of models to predict high-frequency, climate-driven variation in ring widths.

The comparison of observed versus predicted site chronologies was restricted to sites with 10 or more samples, which unfortunately discards all but two FIA sites. Focusing on the ability of each model variant to predict high-frequency, climate-driven variation in ring width, we divided each observed raw ring-width time series by the growth curve predicted by the baseline model (including all fixed and random effects), holding all time-varying climate variables (CAs) constant at their site-specific median. This is analogous to the standard dendrochronological practice of detrending. Predicted ring-width time series were generated with the same model, with a constant stem radius of 17 cm (the median cumulative radius in our dataset) and including interannual climate variability (CAs). Before averaging these observed and predicted time series with Tukey's bi-weight robust mean to form separate site-level chronologies, each was divided by its mean to prevent low-frequency distortions in the site-level chronology due to potential changes in sample replication over time.

The first step in regional-scale model-observation comparison was the delineation of climatically meaningful and geographically coherent regions. Tree-ring time series were clustered into 15 regions using a supervised self-organizing map algorithm (Wehrens & Buydens, 2007), where the inputs were the spline-detrended ring-width time series between 1931 and 1985 (22,000 of 30,388 samples), geographic coordinates (latitude, longitude, and elevation), and climate normals of four variables selected after performing a principal component analysis (PCA) of climate variability across Douglas-fir's entire geographic distribution. The PCA used the 19 Worldclim bioclimatic variables (world clim.org, Fick & Hijmans, 2017), calculated from climate means extracted for each of the 2,699 sites from ClimateNA over the period 1902–2010 (using the R package *dismo*; Hijmans, Phillips, Leathwick, & Elith, 2017) and normalized prior to the PCA. PCA was implemented using the R package *ade4* (Dray & Dufour, 2007), with distance weights proportional to the mean distance of a plot to all other plots so that locations that are more distant from others received greater weight in the analysis. The first three principal components (PC) explained 83% of climate variation across the 2,699 sites. PC1 (41%) was strongly correlated with mean minimum temperature of the coldest month (r = .95). PC2 (30%) was explained by both mean precipitation of the driest quarter and mean diurnal temperature range (r = .92). PC3 (12%) was correlated with variation in mean precipitation of the warmest quarter and mean maximum temperature of the warmest month (r = .89). Out of this PCA, temperature of the coldest month (as a substitute for PC1), PC2, PC3, as well as MAP were selected to represent spatial climatic variation across Douglas-fir's range and entered into the SOM analysis. Strong weighting was necessary to form geographically coherent regions (shown in Figure 2): 40% ring width, and 60% geographic and climate information.

Pearson's correlation coefficients between (regional-scale aggregated) observed versus predicted ring-width time series were then calculated for each region, following the same procedure described above for the site-level analysis. In the ALL-W model variant, time

series were first averaged to form a site-scale chronology and then averaged into a regional-scale chronology, giving greater weight to FIA samples in influencing the regional-scale pattern of radial tree growth.

Finally, we complemented Pearson correlations with calibration-verification trials using a split-period approach for model evaluation. For this, we divided the dataset into two equal halves spanning 1902–1958 and 1959–2016 and parameterized all three model variants over these periods. Reduction of error (RE) and coefficient of efficiency (CE) statistics were used to evaluate prediction (Cook, Briffa, & Jones, 1994), where values <0 indicate limited predictive skill and hence low confidence in model predictions. Model validation at the site and region scales was restricted to periods with sample replication of at least 10 samples per site and 200 samples per region (or 10 sites per region in the ALL-W model variants), respectively.

To visualize the climate sensitivities estimated by the model, we calculated the relative sensitivity of radial growth increments to a change in each variable $\boldsymbol{CA_j}$ (cumulative precipitation or mean maximum temperature) for each 2- (or 3-) month season $\boldsymbol{k}$ by increasing the focal $\boldsymbol{CA_{j,k}}$ by one locally defined standard deviation over the 1902–2010 period, holding all other $\boldsymbol{CA_{j,k}}$ values as well as tree size (*TS*) constant at their median. Thus, we examine the climate sensitivity of Douglas-fir growth in terms of responses to realistically occurring climatic variation at each sampling location in each season.

2.5 | Projection of future growth

We projected future growth of an average-sized tree based upon the fixed effects portion of the generalized mixed-effects models described above. Because we found that average ring width (i.e., productivity) increased with increasing MAT, whereas ring widths declined in response to warmer-than-average years across the majority of Douglas-fir's distribution in most seasons (see Section 3), we considered spatial and temporal variation in climate sensitivity, but not productivity, to be substitutable. In so doing, we presume that climate sensitivities in a warmer future are approximated by climate sensitivities at warmer locations today, whereas productivity is assumed to be no greater (or lesser) than it is today (see Section 4). Operationally, this was achieved by including projected future values of $\boldsymbol{CA_{j,k}}$ in the model and only including projected future values of $\boldsymbol{CNW_i}$ in the interaction terms ($\boldsymbol{\beta_{5i,j,k}}$ and $\boldsymbol{\beta_{7j,k}}$) that capture how the species-wide sensitivity to each $\boldsymbol{CA_{j,k}}$ ($\boldsymbol{\beta_{3j,k}}$) is modified by location in climate space ($\boldsymbol{CNW_i}$). Model projections used near-term (2011–2040) future values of $\boldsymbol{CNW_i}$ and $\boldsymbol{CA_{j,k}}$ variables. Projected changes in growth were calculated as a percent change compared to 20th century mean growth rate at each sampling location, hence we report *relative* growth change. To compare stable (i.e., uniformitarian) and changing climate sensitivities, we compared projected future tree growth using future data for $\boldsymbol{CNW_i}$ versus the 20th century climate normals in $\boldsymbol{CNW_i}$.

For each model variant, projection uncertainty was calculated as the square root of the sum of two subcomponents of uncertainty: (a) the squared 95% prediction interval of the fixed effects part of the model, the fixed effects uncertainty (FEU), as calculated by the R package *merTools* (Knowles & Frederick, 2019) and (b) the squared standard deviation of projections based on the 16 AOGCM runs (SDP).

$$\text{Projection uncertainty} = \sqrt{\text{FEU}^2 + \text{SDP}^2}. \quad (2)$$

While this does not represent a full accounting of projection uncertainty (sensu Dietze, 2017), it quantifies two important sources of uncertainty regarding changes in growth of Douglas-fir: parameter uncertainty and driver uncertainty.

3 | RESULTS

3.1 | Predicted mean ring widths and growth variability

All models performed well at capturing gradients of productivity across the geographic distribution of Douglas-fir. Model-predicted mean ring widths compare well with site index at U.S. Forest Service FIA plots across the U.S. portion of Douglas-fir's distribution (Figure 3b). Highest mean growth rates were predicted at warm and wet sites along the coast from California to Oregon (Figure 3a). With decreasing MAT and MAP, the models predicted smaller growth rings—the smallest in the cold, high-elevation, and dry northern Rocky Mountains in Montana.

The models also revealed geographic variation in interannual growth variability. Regional-scale growth variability, that is, the coefficient of variation (CV) of both observed and predicted regional chronologies, was highest in the southwestern U.S. and declined with increasing MAP, hence lowest in the Olympic Peninsula (Figure 3c). All model variants had high predictive skill at replicating this observed regional-scale trend in CV, with explained variances between 0.76 and 0.89 (Figure 3d). Models predicted noticeably lower growth variability when each sampling location was given equal weight (ALL-W model) compared to predicted growth variability when each time series was given equal weight (ALL model; Figure 3d, $p < .01$, paired *t* test), and even lower variability when only FIA data were used. These differences were especially noticeable in the geographic regions with the highest observed CV, that is, the semiarid southwestern U.S.

3.2 | Calibration and verification

Correlations between observed and modeled ring-width time series increased systematically from the tree to site to region scale, without a clear "best" model among the three model variants. At the tree scale, the average correlation between predicted and observed ring-width time series ranged from 0.40 to 0.41 (*SD*: 0.18–0.21) across all three model variants. At the scale of a sampling

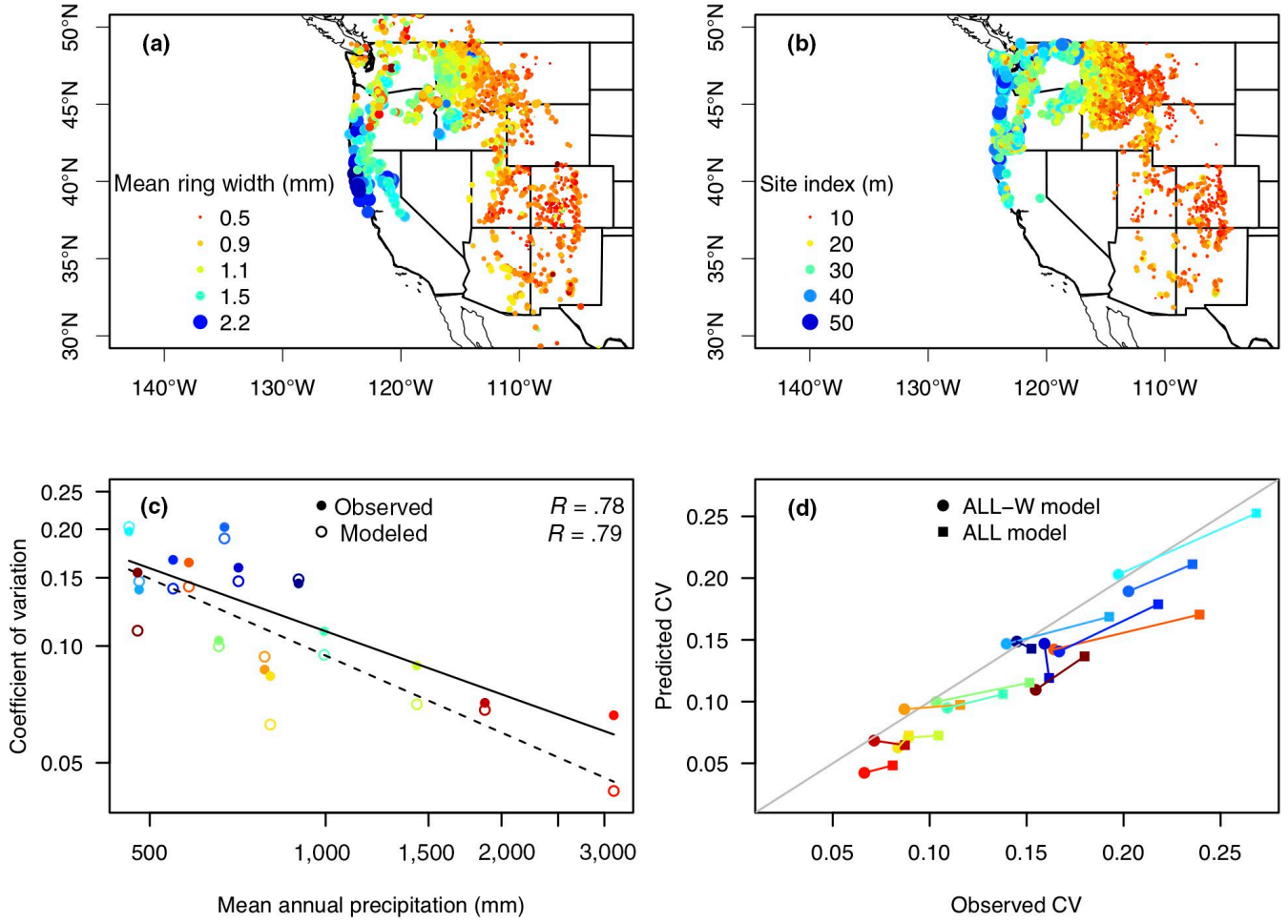

FIGURE 3 Predicted mean radial growth rates from the ALL-W model (a) and site index at base age 50 as estimated in the U.S. FIA program (b). Colors and point sizes range from low (red, small) to high (blue, large) site index or growth rates. (c) Observed (filled points) and modeled (open points, ALL-W) coefficient of variation (CV) of regional-scale chronologies against mean annual precipitation sums. (d) Effect of downweighting highly replicated sites on CV with squares (circles) showing values based on the ALL (ALL-W) model. Colors in (c) and (d) represent the same 15 different regions as color coded in Figure 9

site, the average correlation between predicted and observed time series was 0.45 (±0.20) for the ALL and ALL-W models. Correlations between observed and predicted ring widths were much higher after aggregation to a regional scale. Based only on the FIA data, these correlations ranged from r = .51–.88, with correlations r > .70 in 8 out of 10 regions in the U.S. (regions containing FIA data). Only the two Pacific Northwest regions (Cascades and Olympic Peninsula) had correlations r < .70. When model parameterization relied on all data, the median of the correlations between observed and predicted regional-scale ring-width chronologies was 0.76 in the ALL-W model, and 0.79 in the ALL model (range: r = .47–.86; Figure 4).

In 12 out of 15 regions, both split-period calibration-verification trials passed (i.e., RE and CE > 0) in both models that relied upon the full dataset for parametrization (Table S1). Verification statistics failed (CE < 0) in the Olympic Peninsula (Interior B.C.; northern mid-elevation Rockies) in four (three; two) trials, respectively (Table S1). All eight regions that had sufficient site replication in the FIA model passed the calibration-verification tests (Table S2).

3.3 | Predicted sensitivity of growth to climate variation

Across all model variants, warmer-than-average temperatures tend to negatively impact Douglas-fir ring width (Figure 5), whereas the effect of increased precipitation is positive (Figure 6). There are, however, notable seasonal and geographic variations on this theme. Previous summer and fall temperatures (June–September) showed the strongest negative impacts in the northern interior region, weakening southward (Figure 5a,b). Warmer-than-average cool-season temperatures (October–February) showed the most pronounced negative impacts in the southern extent of Douglas-fir's distribution (Arizona, New Mexico, and Mexico), whereas they positively impacted tree growth in the coastal region and higher-elevation parts of the Rocky Mountains (Figure 5c,d). The sensitivity of Douglas-fir growth to spring temperatures (March and April) showed a strong gradient from positive in the northern interior and high-elevation locations and in California to negative in the U.S. Southwest and Washington state (Figure 5e). Warmer-than-average early summer

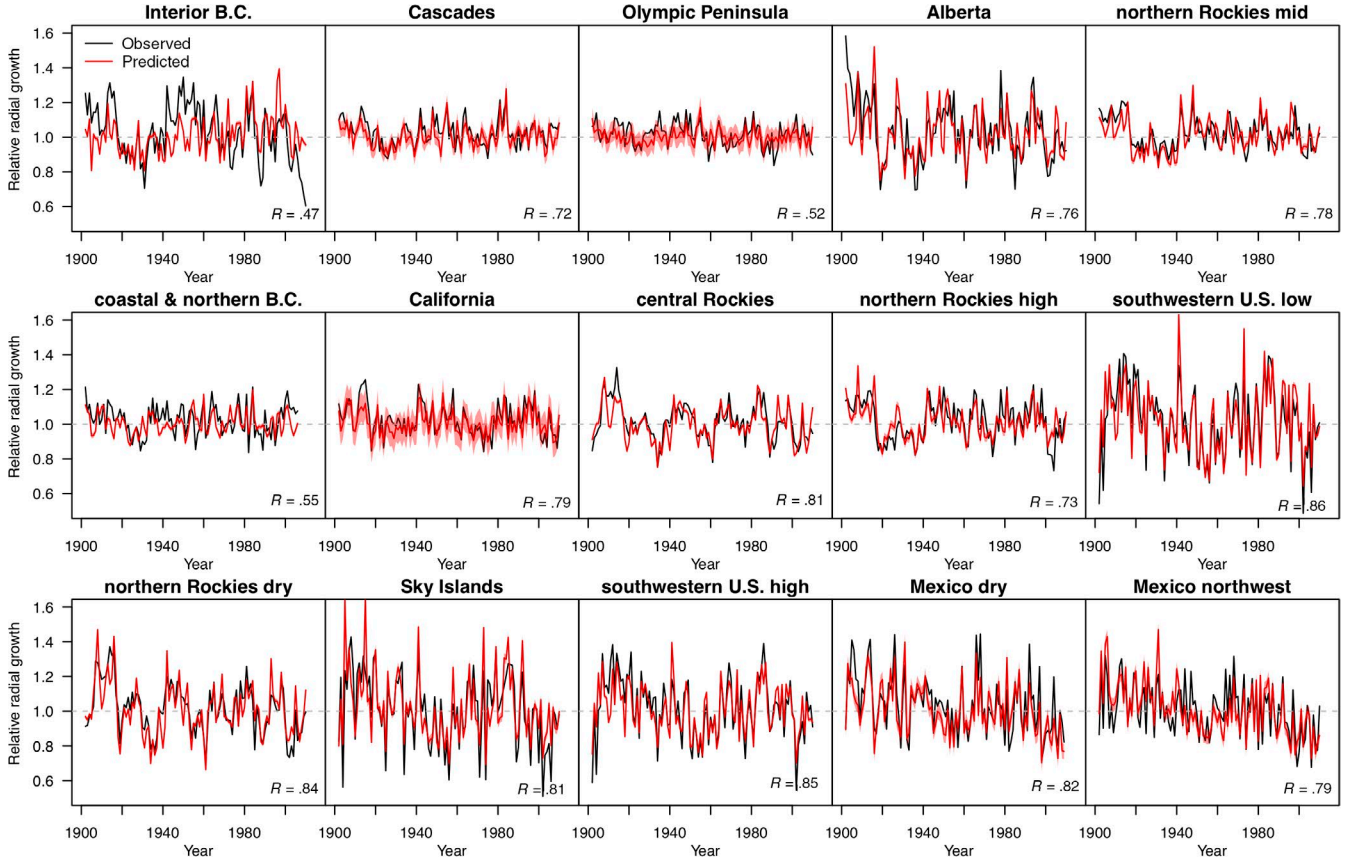

FIGURE 4 Observed (black) and modeled (red) chronologies of the 15 climatic-geographic regions, based on the ALL-W model. Red shading around modeled chronologies shows the 95% prediction interval arising from uncertainties in the fixed effects. Chronologies were cut off when site replication dropped below 10

temperatures (May and June) negatively influenced growth throughout Douglas-fir's range, with the weakest effects in high-elevation parts of the Rocky Mountains (Figure 5f). Mid-summer temperatures (July and August) showed a gradient from negative effects in the northern interior region to positive effects in the domain of the North American Monsoon (Figure 5g).

The impact of previous summer and fall precipitation on Douglas-fir growth was mostly positive (Figure 6a–c). Sensitivity to winter precipitation (December–February) was most positive in Arizona, whereas it was slightly negative west of the Cascades and at high-elevation sites in the northern Rockies (Figure 6d). Spring precipitation (March and April) was most influential in the U.S. Southwest (Figure 6e). Early summer precipitation (May and June) had the strongest positive effects on ring-width increment overall (considering Douglas-fir's range in total; Figure 5f). Mid-summer precipitation exerted the strongest positive influence in the domain of the North American Monsoon, that is, northwestern Mexico and southern Arizona and New Mexico. The more intense colors of Figure 6 compared to Figure 5 highlight also that Douglas-fir radial growth is more sensitive to interannual variability in precipitation than to temperature. Notably, climate sensitivities were weakest in magnitude when only the forest inventory-derived time series were analyzed (FIA model; Figures S1 and S2), and strongest when all data were analyzed weighting each time series equally (ALL model; Figures S3 and S4).

We found a cluster of unusually positive random effects (>0.21; the top 97.5th percentile) for annual precipitation anomalies (site-to-site variation in precipitation sensitivity unexplained by variation in mean climate) across the eastern half of the Colorado Plateau in southern Colorado and northern New Mexico (Figure 7). Considering the interquartile range (IQR) of these random effects (−0.040 to 0.039), these sites were clearly outliers with respect to expected precipitation sensitivity (>1.5 times the IQR).

3.4 | Growth projection

All model variants projected a decline in growth at the majority of sites, compared to the 1902–2010 mean. The smallest relative growth decreases were projected for the Pacific Northwest, and the largest across the dry interior parts of Douglas-fir's distribution, from northwestern Mexico to Alberta, with notable variation on this geographic pattern depending on the model variant. Based on the ALL-W model (Figures 8a and 9), regional median growth was projected to decline in the period 2011–2040 (median: −13%; IQR: −9 to −21), ranging from −5% (IQR: ±0% to −10%) across coastal and northern B.C. to −30% in northwestern Mexico (IQR: −27% to −34%). Using all the data and weighting each time series equally (ALL model, Figure S5a), regional median projected growth changes were

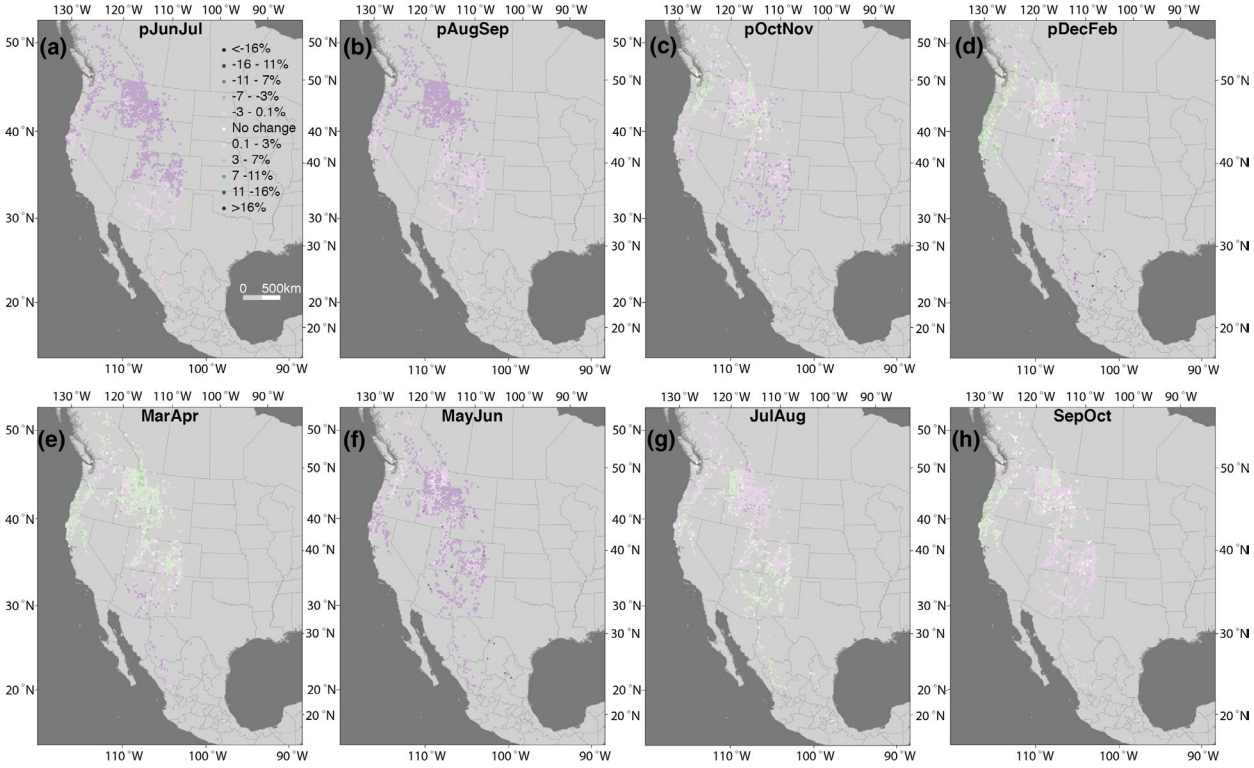

FIGURE 5 Sensitivity of Douglas-fir growth to seasonal maximum temperatures (ALL-W model). Increased growth in response to an increase in temperature of one standard deviation that is locally defined is shown in green; negative changes are violet. Panels (a) to (h) show responses for the eight different seasons of model variable CA_{1k}

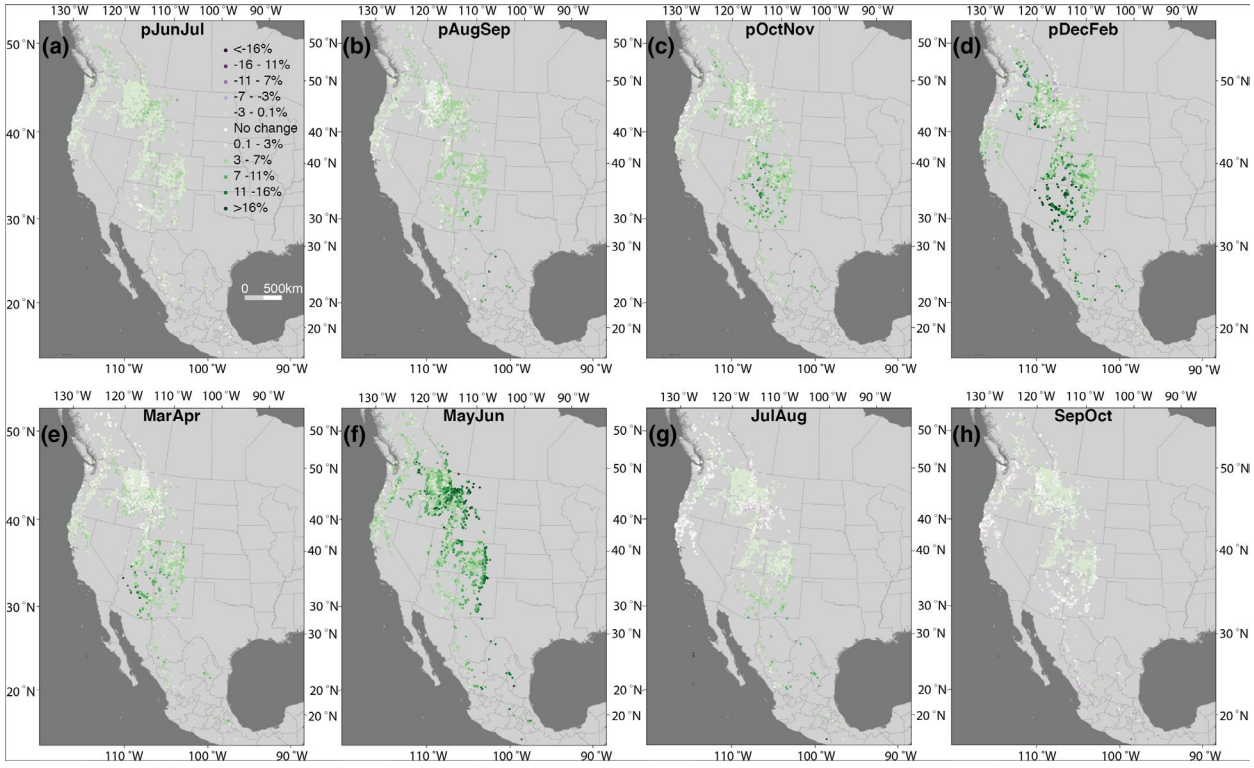

FIGURE 6 Sensitivity of Douglas-fir growth to cumulative precipitation (ALL-W model). Increased growth in response to a locally defined, one standard deviation increase in seasonal cumulative precipitation is shown in green; negative changes are violet. Panels (a) to (h) show responses for the eight different seasons of model variable CA_{2k}

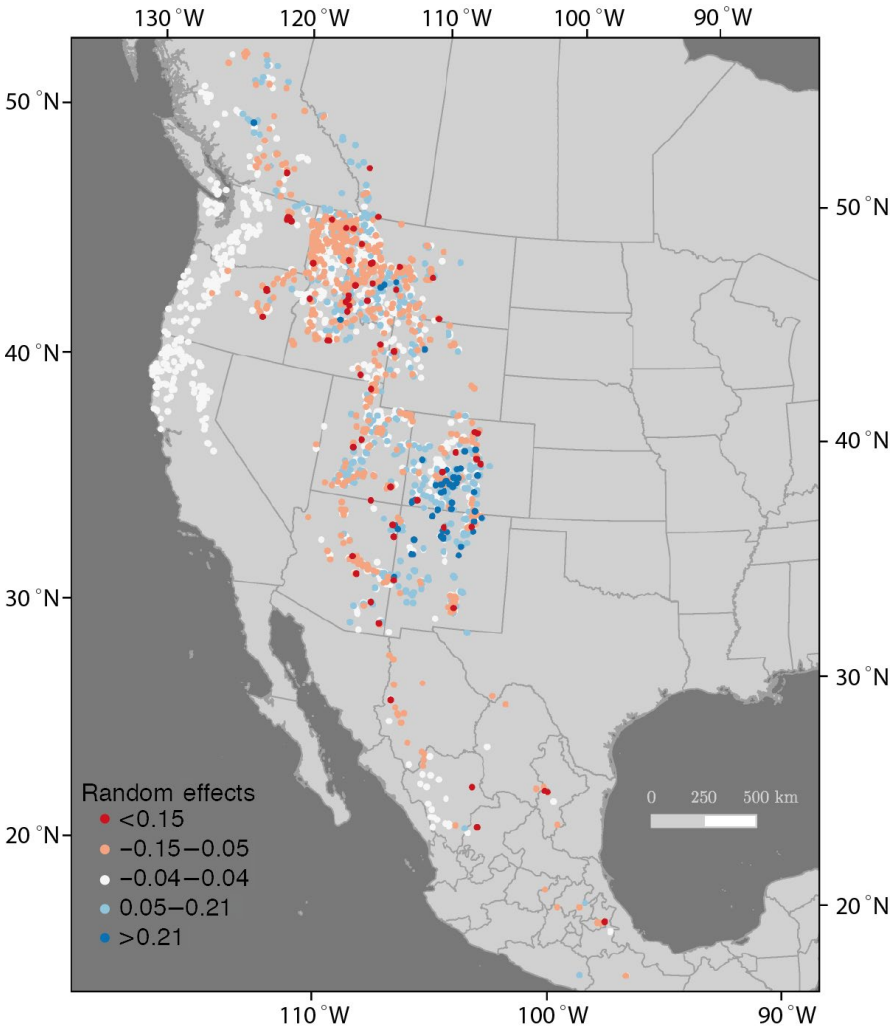

FIGURE 7 Random effects (slope modifications) capturing variation among sites in the effect of annual cumulative precipitation as predicted by the ALL-W model. Blue (red) colors indicate positive (negative) effects, meaning sites are more (less) sensitive to total water-year precipitation than the fixed effects model structure predicts from climate normals. White colors denote values within the interquartile range of the random effects. The pale-colored groups show the 2.5th to 25th (red) and 75th to 97.5th percentile (blue). The two intense-colored groups denote the most extreme values of the random effects

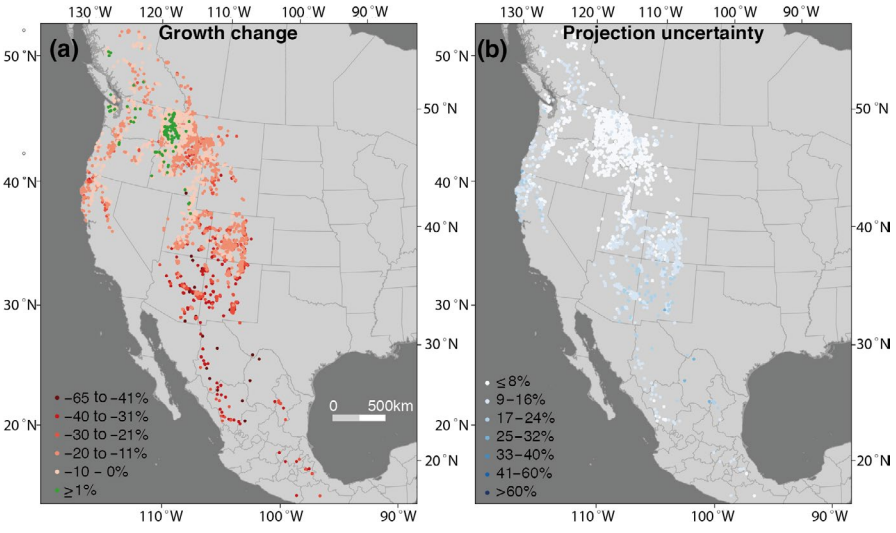

FIGURE 8 (a) Relative growth changes in the ALL-W model for the 2011–2040 period compared to 1902–2010 mean growth rates. Red (green) colors indicate negative (positive) growth changes. Panel (b) shows the full model uncertainties from low (white) to high (blue)

overall slightly stronger (median: −15%; IQR: −8 to −21) and ranged from −5% (IQR: −2% to −9%) in coastal and northern B.C. to −23% (IQR: −16% to −30%) in California and the low-elevation southwestern U.S. Using only the FIA data, the model projected very similar growth decreases (median: −15%; IQR: −10% to −19%; Figure S6a).

We found notable differences in future growth when comparing projection that assumed changing climate sensitivities (the default parameterization) against projection that assumed no change in climate sensitivity (Figure 9). Not accounting for changing climate sensitivities underestimated growth reduction at the warmest and driest

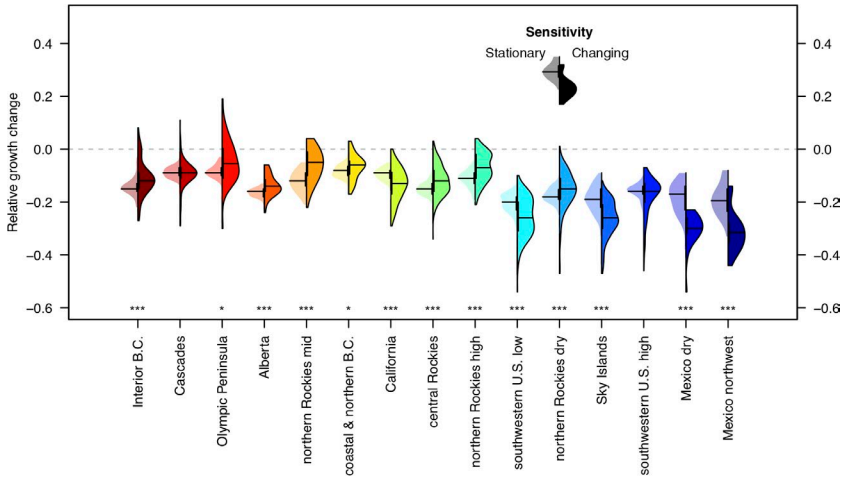

FIGURE 9 Kernel density distributions of regional projected relative growth changes in the ALL-W model assuming temporally stationary climate sensitivity (left) as opposed to the model with changing climate sensitivities (via space-for-time substitution; right) for the 2011–2040 period compared to 1902–2010 mean growth rates. Asterisks denote significant differences in growth changes between the models, where $^{*}p < .05$, and $^{***}p < .001$ using the two-tailed Wilcoxon rank test. Horizontal black lines represent the median of the distributions

sites in the southwestern U.S. and Mexico. At the same time, the approach of assuming constant climate sensitivities (uniformitarianism) did not project positive growth changes in the coolest and wettest regions, such as the Olympic Peninsula and the northern Rockies.

3.5 | Model uncertainties

Across all model variants, model uncertainties were largest in the mesic, coastal portion of Douglas-fir's range. This was especially true when only the FIA data were analyzed. Full projection uncertainties, including both fixed effects uncertainty and uncertainty that arose from variation among the climate projections, varied from ±6% in the central Rockies to ±40% on the Olympic Peninsula (Figure S6b) for the FIA model. Most of the uncertainty arose from the fixed effects uncertainties, which, at ±30%–39% in the Pacific Northwest, was considerably larger than fixed effects uncertainties when all data were analyzed.

Including all data in the analysis and weighting sites equally (ALL-W model) led to lower overall model uncertainty compared to weighting each time series equally (ALL model). Based upon the ALL-W model, regional median fixed effects uncertainties averaged ±2% and ranged from ±1% in Colorado to ±8% in California. Uncertainties that stemmed from differences in AOGCMs ranged between ±3% and ±13%. This led to overall uncertainties in projected growth changes between ±4% in the low-elevation northern Rockies to ±12% in northwestern Mexico and the southwestern U.S. (Figure 8b).

Uncertainties based on the ALL model were notably higher compared to the ALL-W model with roughly twice as high fixed effects uncertainty. This is most evident in the coastal portion of Douglas-fir's distribution, that is, comparing Figure 8b with Figure S5b.

4 | DISCUSSION

Tree rings are a powerful tool to investigate past climate. Projection of future tree growth is an obvious extension of the same logic, with one problem: the future will not look like the past. Specifically, the climate sensitivity of tree growth at any one location under future (warmer) conditions is expected to increasingly differ from the climate sensitivity of tree growth at that location in the past. Here, we evaluate the expectation (from Fritts et al., 1965) that average ring width and climate sensitivities are variable across environmental space in a predictable fashion. We then address the appropriateness of using SFTS to anticipate the response of tree growth to future climate conditions.

4.1 | Climate sensitivity and productivity are predictable

The model infers widespread positive sensitivity to precipitation (Figure 6), corroborating numerous regional studies in the U.S. Southwest (Adams & Kolb, 2005; Fritts et al., 1965), the Pacific Northwest (Beedlow, Lee, Tingey, Waschmann, & Burdick, 2013; Case & Peterson, 2005; Littell et al., 2008; Lo et al., 2010; Zhang & Hebda, 2004), and the northern limit of the species' distribution in B.C. and Alberta (Griesbauer & Green, 2010a, 2010b; Lo et al., 2010; Razavi et al., 2015; Watson & Luckman, 2002). Water-limited growth is further evidenced by negative effects of warmer-than-average temperatures (Figure 5), presumably because increased evapotranspiration exacerbates drought stress (Bréda, Huc, Granier, & Dreyer, 2006; Vicente-Serrano, Beguería, & López-Moreno, 2010; Williams et al., 2013). There were two times and places where warmer temperatures benefited tree growth. First, the positive sensitivity to March and April temperatures found from the central Rockies to northern B.C. (Figure 5e) suggests beneficial effects of earlier snow melt and a longer growing season (Case & Peterson, 2005; Pederson et al., 2011; Peterson, Peterson, & Ettl, 2002). Second, we found positive sensitivity to July–August temperatures in western Mexico and the Sky Islands. During these months, heat stimulates evaporative moisture supply to the North American Monsoon and thus increase precipitation from convective thunderstorms so that instead of intensifying drought stress, warmer temperatures may increase

stomatal conductance, and stimulate enzymatic activity and cell production (Belmecheri, Wright, Szejner, Morino, & Monson, 2018; Parent, Turc, Gibon, Stitt, & Tardieu, 2010; Urban, Košvancová, Marek, & Lichtenthaler, 2007).

With respect to productivity, the model infers radial growth increments are greatest in the coastal, warm-mesic portion of Douglas-fir's distribution where climate sensitivities are weakest. Moving away from this "niche optimum," there are two dimensions in which climate becomes limiting to Douglas-fir growth: temperature and precipitation. The smallest ring widths are found where these two limiting factors combine, for example, high-elevation (cold), continental (dry) sites in the northern Rocky Mountains of Montana. Our estimates of average growth rates mirror the spatial pattern of growth potential indicated by a forest inventory site index (Figure 3a,b, Weiskittel, Crookston, & Radtke, 2011). From Fritts et al. (1965), we expected to find these opposing patterns of productivity and climate sensitivity (see Figure 1) and it is encouraging that they indeed turned out to be predictable across environmental and geographic space.

4.2 | Partial space-for-time substitution, an (im) perfect solution

Given that productivity and climate sensitivity are predictable, can SFTS be used to anticipate how a tree at a cooler location today will grow in a warmer future? Inferred effects of spatial versus temporal variation in temperature had opposite signs (see also Canham et al., 2018). Trees at warmer locations have larger growth increments, even though the sensitivity to interannual variation in temperature is almost universally negative. Applying SFTS to Douglas-fir's productivity and climate sensitivity would lead to the prediction that trees responding negatively to warmer-than-average temperatures will grow more in a warmer future, eliciting a closer examination of the assumptions underlying SFTS. Two important assumptions of SFTS are that (a) the processes responsible for spatial and temporal variation are the same and hence (b) there is no mismatch in time scale between these drivers. Observed spatial variation in Douglas-fir productivity and climate sensitivity are partly the product of evolutionary adaptation (i.e., have a genetic basis), whereas the change in growth we wish to predict—future growth compared to historical growth—is driven by rapid anthropogenic climate change. Evolution is a slow process in long-lived organisms such as trees, compared to the pace of anthropogenic climate change (Gugger, Sugita, & Cavender-Bares, 2010). Filling in the unknown behavior of future trees by presuming they will behave exactly as trees of different, locally adapted genotypes at another location today clearly violates the assumptions underlying SFTS.

While we argue against using spatial variation in both productivity and climate sensitivity to anticipate future tree growth, substitution of climate sensitivities alone may yield a first-pass approximation of the response to future climate. The process of local adaptation produces not only different growth rates achieved by different genotypes across spatial environmental gradients but also adaptive plasticity in response to strictly temporal environmental variation. The latter is visualized in terms of a reaction norm (Schlichting, 1986; Via & Lande, 1985). Here we have estimated reaction norms as a simple linear response, captured by the species-wide sensitivity to each $\boldsymbol{CA}_{j,k}$ ($\boldsymbol{\beta}_{3j,k}$) and how it is modified by location in climate space ($\boldsymbol{CNW}_i$) through the interaction terms ($\boldsymbol{\beta}_{5i,j,k}\boldsymbol{CNW}_{i,p,t} * \boldsymbol{CA}_{j,k,p,t}$ and $\boldsymbol{\beta}_{7i,j,k}\,CNW_{1,p,t} * CNW_{2,p,t} * \boldsymbol{CA}_{j,k,p,t}$). But instead of a linear response, reaction norms should be curved such that climate sensitivity increases as climate deviates from its historical mean and variance and becomes increasingly limiting to tree growth. Indeed, spatial variation in climate sensitivities inferred by the model shows that with warmer temperatures (MAT), the sensitivity of ring widths to temperature becomes increasingly negative (Figure 5). The use of today's warmer-location climate sensitivities to stand in for future climate sensitivities is thus a conservative estimate of how tree growth may decline with warming temperatures—it assumes that the in situ genotype responds exactly as another genotype elsewhere would respond. While a 1:1 substitution of climate sensitivities might not be perfect, it is certainly better than assuming that trees will respond to future climate in the same way that they have responded to past climate—that is, the assumption of uniformitarianism.

Ultimately, to better anticipate the future growth of trees, it will be necessary to parse the effects of genotype, environment, and their interaction on growth (Marchal et al., 2019). We are unable to disentangle how much of the spatial variation observed here (in productivity and climate sensitivities) is caused by genetic versus environmental differences because the data do not have a reciprocal common garden design. In particular, it is possible that geographic variation in productivity has a greater basis in heritable variation (rather than plasticity), whereas geographic variation in climate sensitivities has a greater basis in plasticity (rather than heritability), which would further justify the substitutability of climate sensitivities (and not productivity). Many common garden studies of trees show that different provenances react very similarly to interannual climate variability when growing at the same site but grow at very different rates (e.g., Isaac-Renton et al., 2018; Leland et al., 2016; Montwé, Isaac-Renton, Hamann, & Spiecker, 2016; Montwé, Spiecker, & Hamann, 2015; Taeger, Zang, Liesebach, Schneck, & Menzel, 2013), but to our knowledge, the genetic versus plastic basis of productivity compared to climate sensitivity has not been quantified. A further challenge is that non-climatic environmental drivers of spatial variation in growth (soil type, land-use legacies, stand age and structure, etc.) cannot be distinguished from climatic drivers without additional covariate information. It is even possible that some of these non-climatic drivers might be collinear with climate (e.g., soil organic matter content may covary with mean annual temperature or precipitation). In other words, the climate sensitivities (regression coefficients β_2, β_4, β_6, and β_8) estimated by our model would falsely conflate climate with other non-climatic factors that cannot change as rapidly as climate. Finally, to the degree that growth differences have a plastic basis, adjustments in tree height, leaf area index, and even forest stand-level characteristics may mitigate climate-driven declines in performance (growth).

4.3 | Growth projection

Implementing partial SFTS, growth declines are projected across nearly the entire distribution of Douglas-fir (Figure 8a), as a consequence of widespread negative temperature sensitivity and associated water limitation on growth (Restaino et al., 2016). This result is consistent with previous projections (Charney et al., 2016; Chen, Welsh, & Hamann, 2010). The strongest projected growth reductions across all model variants were in the dry and warm parts of the Interior West and the weakest reductions in the Pacific Northwest. We found the potential for growth increases in the near future in the wettest and coldest regions (Olympic Peninsula, Cascades, northern & coastal B.C., and high-elevation northern Rockies; Figure 9). In those regions, the growth projection suggested the benefits of warmer conditions combined with a longer growing season may outweigh the negative effects of increased drought stress; it is difficult to predict how long this positive effect may last, that is, how soon a positive response may change to a negative response, moving from the left to the right in Figure 1. Concurrently, heat and drought stress-related growth decreases are projected at the warm-dry edge of Douglas-fir's distribution, that is, the semiarid southwestern U.S., possibly further accelerating associated tree mortality (Adams et al., 2017). Not accounting for changing climate sensitivities, we would underestimate the negative impacts at Douglas-fir's warm-dry edge and simultaneously miss possible beneficial effects of climate change in its climate optimum (Figure 9).

The regional pattern of growth decline was largely consistent across the three model variants. It is important to note that all projections of future growth are expressed as a percentage of historical ring widths so that small relative growth changes projected in the mesic, coastal portion of Douglas-fir's distribution may actually have a larger impact on absolute biomass accumulation (i.e., carbon sequestration) compared to the larger relative decline in Douglas-fir stands in the U.S. Southwest, where productivity is much lower.

At the same time, model fits were poorest and projection uncertainties highest in the coastal mesic region, including lower correlations between observed and model-predicted ring-width, and lower RE and CE statistics, especially at locations close to the coast. There were two reasons for these poor model fits: weak climate sensitivity in this most productive part of the species' distribution, combined with sparse data. Notably, we were able to gather only 4,367 tree-ring time series for the coastal variety of Douglas-fir, compared to 26,021 time series for the interior variety. These two factors together, perniciously, create a low signal-to-noise ratio. Fixed effects uncertainties were high in the productive coastal areas and might not represent climate sensitivities sufficiently well to reliably project future tree growth (Figure 8; Figures S5 and S6). In contrast, fixed effects parameter uncertainty and projection uncertainty were comparatively low across the Interior West. In Arizona, for example, there were only 119 samples from 94 FIA sites, but projection uncertainties were almost as low as when all data were used (compare Figure S6 with Figure 8 and Figure S5). Interestingly, uncertainties along the coast were much lower when sampling sites were given equal weight (ALL-W model; Figure 8) compared to weighting all time series equally (ALL model; Figure S5), suggesting that in a relatively data-sparse and heterogeneous region such as California, model uncertainty is more driven by spatial coverage than by sample replication per site.

4.4 | Advantages of mixed-effects modeling

A range-wide, tree-level mixed-effects modeling approach has several advantages over traditional site-by-site analyses. First, this makes it possible to use data that would never meet standard dendrochronological criteria for chronology building (i.e., low replication per site in the FIA dataset). Second, the model captures how tree size and climate influence ring-width variation while accounting for additional relevant but unquantified factors. For example, the model did not explicitly include any stand-related information (e.g., stand density) or site-level differences influencing soil moisture or nutrients. With tree random effects nested within site random effects, a mixed-effects (or "hierarchical") model is robust against these additional influences. Two examples illustrate this: First, in Interior B.C. (Figure 4), where observed ring widths were very small in the 2000s, model-predicted ring widths did not track these observed declines. Many of the chronologies from this area were collected in stands affected by western spruce budworm defoliation (Alfaro, Berg, & Axelson, 2014; Axelson, Smith, Daniels, & Alfaro, 2015; Harvey, Axelson, & Smith, 2018). In a site-by-site (or even region-by-region) analysis, those years of reduced growth would have exerted a greater influence on estimates of climate sensitivities compared to an analysis that considers climate variability across the distribution of Douglas-fir.

A second example is a noticeable cluster in southern Colorado and northern New Mexico of strongly positive random effects modifying the predicted sensitivity to MAP (Figure 7). These sampling locations are unusually sensitive to variation in annual precipitation, relative to what the model predicts based on the fixed effects information from the larger data network. Most of these time series were ITRDB locations used for reconstructing hydroclimate, suggesting that dendrohydrologists were indeed successful in choosing sites and trees that were extremely sensitive to precipitation variability.

An additional advantage is that our model represents a continuous implementation of SFTS compared to the discrete grouping approach used by Charney et al. (2016), in which climate sensitivities changed only after entering another bioclimatic zone. As a consequence, our model depicts small-scale variation in climate responses due to rain shadow effects and variation in elevation. This leads to a more heterogeneous picture of possible growth changes for the 2011–2040 period across the entire range of Douglas-fir (Figures 8 and 9). For example, across the arid U.S. Southwest, a small fraction of sites had modeled growth decreases of only 12%–18% (90–100th percentile), whereas at the least favorable locations, growth is expected to decrease by 35%–47% (0–10th percentile).

4.5 | Back to the future

Simultaneously modeling size- or age-growth and climate–growth relationships across space within a flexible analytical framework (mixed-effects models) is a recent development in dendroecology (e.g., Canham et al., 2018; Martin-Benito et al., 2011; Martínez-Vilalta et al., 2012; Redmond et al., 2017). Yet, it represents a return to a fundamental, but underappreciated cornerstone of dendrochronology—Cook's (1987) aggregate growth model. We can continue to improve the projection of future tree growth by further fleshing out Cook's aggregate model, moving some of the tree- and site-level influences that were treated as random effects here into the list of fixed effects: tree genotype, biophysical site characteristics, forest stand conditions, and the influences of disturbances like fire and insects. Such multiple regression modeling will require more and better covariate data, which are routinely collected in forest inventories or permanent sample plots.

Yet, increment core collection in forest inventory programs has thus far been mostly ad hoc. While the FIA annual program was designed to be geographically and temporally representative of forested conditions across the U.S., the sampling of increment cores is not yet well enough replicated in the climate optimum of Douglas-fir (the coastal, warm-mesic domain), and lacks representation during the last ~20 years in the U.S. Southwest, when warming and drought have been most pronounced. Continued collection of increment cores on forest inventory plots is therefore a high priority, both to fill existing data gaps and to enhance our understanding of climate sensitivities as trees continue to experience changing conditions. With continuous input of tree-ring data, and further development of mixed-effects modeling of absolute ring-width variation, it will be possible to iteratively glimpse the future of forest ecosystem functioning, better anticipate forest ecosystem behavior and manage accordingly, in a coupled process of scientific advancement and adaptive management that has been termed "iterative near-term ecological forecasting" (Dietze et al., 2018).

One of the great challenges of global change research is to develop models that successfully simulate ecosystem behavior across scales (Levy et al., 2014). It has been shown that the state-of-the-art, big-leaf photosynthesis-driven DGVMs commonly used in large-scale climate projections (e.g., the TRENDY suite, Sitch et al., 2015) overestimate interannual climate sensitivity, especially (but not only) at the cold and warm edge of the temperate zone (Babst et al., 2013; Klesse, Babst, et al., 2018; Rollinson et al., 2017). This misrepresentation of climate sensitivity and the inability to accurately model carbon allocation to the stem may be indicative of the fact that DGVMs have been historically developed based upon parameterization of leaf-scale processes. The current dataset covering the entire distribution of Douglas-fir (but also tree-ring width records in general) is well-suited to serve as a calibration target or assimilation dataset for improvement in stem growth predictions of next-generation (mechanistic) models of varying complexity (Mina, Martin-Benito, Bugmann, & Cailleret, 2016; Zuidema, Poulter, & Frank, 2018).

ACKNOWLEDGEMENTS

We dedicate this paper to the memory of Hal Fritts (1928–2019), an exceptional observer of trees and great thinker. The authors thank Gregory Pederson, Peter Dunwiddie, Michael Case, Jeremy Littell, Emma Watson, Daniel Ryerson, Tom Swetnam, Chris Baisan, and Qi-Bin Zhang for the data they contributed, along with the many other scientists that contributed to and maintain(ed) the ITRDB. This manuscript is based upon work supported by the National Science Foundation under awards DBI-0735191 and DBI-1265383 (URL: https://www.cyverse.org/). Our thanks go also to Martin Munro and Tyson Swetnam for their technical assistance. SK acknowledges the support of the USDA-AFRI grant 2016-67003-24944; MEKE was supported by the National Science Foundation under award DBI-1802893. FB acknowledges statutory funds from the W. Szafer Institute of Botany PAS, as well as support from the project "Inside out" (#POIR.04.04.00-00-5F85/18-00) funded by the HOMING programme of the Foundation for Polish Science, co-financed by the European Union under the European Regional Development Fund.

DATA AVAILABILITY STATEMENT

The data that support the findings of this study are available from the corresponding author upon reasonable request.

ORCID

Stefan Klesse https://orcid.org/0000-0003-1569-1724
Christopher H. Guiterman https://orcid.org/0000-0002-9706-9332
Ann M. Lynch https://orcid.org/0000-0002-8043-3855
John D. Shaw https://orcid.org/0000-0002-5797-1006

REFERENCES

Adams, H. D., & Kolb, T. E. (2005). Tree growth response to drought and temperature in a mountain landscape in northern Arizona, USA. *Journal of Biogeography*, *32*(9), 1629–1640. https://doi.org/10.1111/j.1365-2699.2005.01292.x

Adams, H. D., Zeppel, M. J. B., Anderegg, W. R. L., Hartmann, H., Landhäusser, S. M., Tissue, D. T., … McDowell, N. G. (2017). A multi-species synthesis of physiological mechanisms in drought-induced tree mortality. *Nature Ecology & Evolution*, *1*(9), 1285–1291. https://doi.org/10.1038/s41559-017-0248-x

Alfaro, R. I., Berg, J., & Axelson, J. (2014). Periodicity of western spruce budworm in Southern British Columbia, Canada. *Forest Ecology and Management*, *315*, 72–79. https://doi.org/10.1016/j.foreco.2013.12.026

Allen, E. B., Rittenour, T. M., DeRose, R. J., Bekker, M. F., Kjelgren, R., & Buckley, B. M. (2013). A tree-ring based reconstruction of Logan River streamflow, northern Utah. *Water Resources Research*, *49*(12), 8579–8588. https://doi.org/10.1002/2013WR014273

Anderegg, L. D. L., & HilleRisLambers, J. (2019). Local range boundaries vs. large-scale trade-offs: Climatic and competitive constraints on tree growth. *Ecology Letters*, *22*(5), 787–796. https://doi.org/10.1111/ele.13236

Axelson, J. N., Smith, D. J., Daniels, L. D., & Alfaro, R. I. (2015). Multicentury reconstruction of western spruce budworm outbreaks in central British Columbia, Canada. *Forest Ecology and Management*, *335*, 235–248. https://doi.org/10.1016/j.foreco.2014.10.002

Babst, F., Bodesheim, P., Charney, N., Friend, A. D., Girardin, M. P., Klesse, S., … Evans, M. E. K. (2018). When tree rings go global: Challenges and

opportunities for retro- and prospective insight. *Quaternary Science Reviews*, *197*, 1–20. https://doi.org/10.1016/j.quascirev.2018.07.009

Babst, F., Bouriaud, O., Poulter, B., Trouet, V., Girardin, M. P., & Frank, D. C. (2019). Twentieth century redistribution in climatic drivers of global tree growth. *Science Advances*, *5*(1), eaat4313. https://doi.org/10.1126/sciadv.aat4313

Babst, F., Poulter, B., Trouet, V., Tan, K., Neuwirth, B., Wilson, R., … Frank, D. (2013). Site- and species-specific responses of forest growth to climate across the European continent: Climate sensitivity of forest growth across Europe. *Global Ecology and Biogeography*, *22*(6), 706–717. https://doi.org/10.1111/geb.12023

Bates, D., Mächler, M., Bolker, B., & Walker, S. (2015). Fitting linear mixed-effects models using lme4. *Journal of Statistical Software*, *67*(1), 1–48. https://doi.org/10.18637/jss.v067.i01

Bechtold, W. A., & Patterson, P. L. (2005). *The enhanced forest inventory and analysis program – National sampling design and estimation procedures. Gen. Tech. Rep. SRS-80*. Asheville, NC: U.S. Department of Agriculture, Forest Service, Southern Research Station, 85 pp., 080. https://doi.org/10.2737/SRS-GTR-80

Beedlow, P. A., Lee, E. H., Tingey, D. T., Waschmann, R. S., & Burdick, C. A. (2013). The importance of seasonal temperature and moisture patterns on growth of Douglas-fir in western Oregon, USA. *Agricultural and Forest Meteorology*, *169*, 174–185. https://doi.org/10.1016/j.agrformet.2012.10.010

Belmecheri, S., Wright, W. E., Szejner, P., Morino, K. A., & Monson, R. K. (2018). Carbon and oxygen isotope fractionations in tree rings reveal interactions between cambial phenology and seasonal climate. *Plant, Cell & Environment*, *41*(12), 2758–2772. https://doi.org/10.1111/pce.13401

Bonan, G. B. (2008). Forests and climate change: Forcings, feedbacks, and the climate benefits of forests. *Science*, *320*(5882), 1444–1449. https://doi.org/10.1126/science.1155121

Bréda, N., Huc, R., Granier, A., & Dreyer, E. (2006). Temperate forest trees and stands under severe drought: A review of ecophysiological responses, adaptation processes and long-term consequences. *Annals of Forest Science*, *63*(6), 625–644. https://doi.org/10.1051/forest:2006042

Canham, C. D., Murphy, L., Riemann, R., McCullough, R., & Burrill, E. (2018). Local differentiation in tree growth responses to climate. *Ecosphere*, *9*(8), e02368. https://doi.org/10.1002/ecs2.2368

Case, M. J., & Peterson, D. L. (2005). Fine-scale variability in growth climate relationships of Douglas-fir, North Cascade Range, Washington. *Canadian Journal of Forest Research*, *35*(11), 2743–2755. https://doi.org/10.1139/x05-191

Charney, N. D., Babst, F., Poulter, B., Record, S., Trouet, V. M., Frank, D., … Evans, M. E. K. (2016). Observed forest sensitivity to climate implies large changes in 21st century North American forest growth. *Ecology Letters*, *19*(9), 1119–1128. https://doi.org/10.1111/ele.12650

Chen, P.-Y., Welsh, C., & Hamann, A. (2010). Geographic variation in growth response of Douglas-fir to interannual climate variability and projected climate change: Douglas-fir growth response to climate change. *Global Change Biology*, *16*(12), 3374–3385. https://doi.org/10.1111/j.1365-2486.2010.02166.x

Cook, E. R. (1987). The decomposition of tree-ring series for environmental studies. *Tree-Ring Bulletin*, *47*, 37–59.

Cook, E. R., Briffa, K. R., & Jones, P. D. (1994). Spatial regression methods in dendroclimatology: A review and comparison of two techniques. *International Journal of Climatology*, *14*(4), 379–402. https://doi.org/10.1002/joc.3370140404.

Cook, E. R., Seager, R., Kushnir, Y., Briffa, K. R., Büntgen, U., Frank, D., … Zang, C. (2015). Old world megadroughts and pluvials during the common era. *Science Advances*, *1*(10), e1500561. https://doi.org/10.1126/sciadv.1500561

Damgaard, C. (2019). A critique of the space-for-time substitution practice in community ecology. *Trends in Ecology & Evolution*, *34*(5), 416–421. https://doi.org/10.1016/j.tree.2019.01.013

de Boor, C. (1978). *A practical guide to splines*. Springer-Verlag. Retrieved from https://www.springer.com/de/book/9780387953663

DeRose, R. J., Shaw, J. D., & Long, J. N. (2017). Building the forest inventory and analysis tree-ring data set. *Journal of Forestry*, *115*(4), 283–291. https://doi.org/10.5849/jof.15-097

Dietze, M. C. (2017). Prediction in ecology: A first-principles framework. *Ecological Applications*, *27*(7), 2048–2060. https://doi.org/10.1002/eap.1589

Dietze, M. C., Fox, A., Beck-Johnson, L. M., Betancourt, J. L., Hooten, M. B., Jarnevich, C. S., … White, E. P. (2018). Iterative near-term ecological forecasting: Needs, opportunities, and challenges. *Proceedings of the National Academy of Sciences of the United States of America*, *115*(7), 1424–1432. https://doi.org/10.1073/pnas.1710231115

Dray, S., & Dufour, A.-B. (2007). The ade4 package: Implementing the duality diagram for ecologists. *Journal of Statistical Software*, *22*(1), 1–20. https://doi.org/10.18637/jss.v022.i04

Fick, S. E., & Hijmans, R. J. (2017). WorldClim 2: New 1-km spatial resolution climate surfaces for global land areas. *International Journal of Climatology*, *37*(12), 4302–4315. https://doi.org/10.1002/joc.5086

Friedlingstein, P., Meinshausen, M., Arora, V. K., Jones, C. D., Anav, A., Liddicoat, S. K., & Knutti, R. (2014). Uncertainties in CMIP5 climate projections due to carbon cycle feedbacks. *Journal of Climate*, *27*(2), 511–526. https://doi.org/10.1175/JCLI-D-12-00579.1

Fritts, H. (1976). *Tree rings and climate*. London, UK: Academic Press.

Fritts, H. C., Smith, D. G., Cardis, J. W., & Budelsky, C. A. (1965). Tree-ring characteristics along a vegetation gradient in northern Arizona. *Ecology*, *46*(4), 393–401. https://doi.org/10.2307/1934872

González de Andrés, E., Camarero, J. J., Blanco, J. A., Imbert, J. B., Lo, Y.-H., Sangüesa-Barreda, G., & Castillo, F. J. (2017). Tree-to-tree competition in mixed European beech-Scots pine forests has different impacts on growth and water-use efficiency depending on site conditions. *Journal of Ecology*, *106*(1), 59–75. https://doi.org/10.1111/1365-2745.12813

Griesbauer, H. P., & Green, D. S. (2010a). Regional and ecological patterns in interior Douglas-fir climate–growth relationships in British Columbia, Canada. *Canadian Journal of Forest Research*, *40*(2), 308–321. https://doi.org/10.1139/X09-197

Griesbauer, H. P., & Green, D. S. (2010b). Assessing the climatic sensitivity of Douglas-fir at its northern range margins in British Columbia, Canada. *Trees*, *24*(2), 375–389. https://doi.org/10.1007/s00468-009-0407-z

Gugger, P. F., Sugita, S., & Cavender-Bares, J. (2010). Phylogeography of Douglas-fir based on mitochondrial and chloroplast DNA sequences: Testing hypotheses from the fossil record. *Molecular Ecology*, *19*(9), 1877–1897. https://doi.org/10.1111/j.1365-294X.2010.04622.x

Guiterman, C. H. (2016). *Climate and human drivers of forest vulnerability in the US Southwest: Perspectives from dendroecology*. The University of Arizona. Retrieved from http://search.proquest.com/openview/037c61cd3b52b7ca5d77752352826230/1?pq-origsite=gscholar&cbl=18750&diss=y

Gustafson, E. J. (2013). When relationships estimated in the past cannot be used to predict the future: Using mechanistic models to predict landscape ecological dynamics in a changing world. *Landscape Ecology*, *28*(8), 1429–1437. https://doi.org/10.1007/s10980-013-9927-4

Harvey, J. E., Axelson, J. N., & Smith, D. J. (2018). Disturbance–climate relationships between wildfire and western spruce budworm in interior British Columbia. *Ecosphere*, *9*(3), e02126. https://doi.org/10.1002/ecs2.2126

Hijmans, R. J., Phillips, S., Leathwick, J., & Elith, J. (2017). dismo: Species distribution modeling (Version R package version 1.1-4) [Computer Software].

Hutchinson, G. E. (1978). *Introduction to population ecology*. New Haven, CT: Yale University Press.

Isaac-Renton, M., Montwé, D., Hamann, A., Spiecker, H., Cherubini, P., & Treydte, K. (2018). Northern forest tree populations are

physiologically maladapted to drought. *Nature Communications*, *9*(1), 5254. https://doi.org/10.1038/s41467-018-07701-0

Isaac-Renton, M., Roberts, D. R., Hamann, A., & Spiecker, H. (2014). Douglas-fir plantations in Europe: A retrospective test of assisted migration to address climate change. *Global Change Biology*, *20*(8), 2607–2617. https://doi.org/10.1111/gcb.12604

Klesse, S., Babst, F., Lienert, S., Spahni, R., Joos, F., Bouriaud, O., … Frank, D. C. (2018). A combined tree ring and vegetation model assessment of european forest growth sensitivity to interannual climate variability. *Global Biogeochemical Cycles*, *32*(8), 1226–1240. https://doi.org/10.1029/2017GB005856

Klesse, S., DeRose, R. J., Guiterman, C. H., Lynch, A. M., O'Connor, C. D., Shaw, J. D., & Evans, M. E. K. (2018). Sampling bias overestimates climate change impacts on forest growth in the southwestern United States. *Nature Communications*, *9*(1), 5336. https://doi.org/10.1038/s41467-018-07800-y

Knapp, A. K., Ciais, P., & Smith, M. D. (2017). Reconciling inconsistencies in precipitation–productivity relationships: Implications for climate change. *New Phytologist*, *214*(1), 41–47. https://doi.org/10.1111/nph.14381

Knowles, J. E., & Frederick, C. (2019). merTools: Tools for analyzing mixed effect regression models (Version R package version 0.5.0) [Computer software]. Retrieved from https://CRAN.R-project.org/package=merTools.

Leland, C., Hom, J., Skowronski, N., Ledig, F. T., Krusic, P. J., Cook, E. R., … Pederson, N. (2016). Missing rings, synchronous growth, and ecological disturbance in a 36-year pitch pine (*Pinus rigida*) provenance study. *PLoS ONE*, *11*(5), e0154730. https://doi.org/10.1371/journal.pone.0154730

Levy, O., Ball, B. A., Bond-Lamberty, B., Cheruvelil, K. S., Finley, A. O., Lottig, N. R., … Williams, J. W. (2014). Approaches to advance scientific understanding of macrosystems ecology. *Frontiers in Ecology and the Environment*, *12*(1), 15–23. https://doi.org/10.1890/130019.

Littell, J. S., Peterson, D. L., & Tjoelker, M. (2008). Douglas-fir growth in mountain ecosystems: Water limits tree growth from stand to region. *Ecological Monographs*, *78*(3), 349–368. https://doi.org/10.1890/07-0712.1

Lo, Y.-H., Blanco, J. A., Seely, B., Welham, C., & Kimmins, J. P. (Hamish). (2010). Relationships between climate and tree radial growth in interior British Columbia, Canada. *Forest Ecology and Management*, *259*(5), 932–942. https://doi.org/10.1016/j.foreco.2009.11.033

Maguire, B. (1973). Niche response structure and the analytical potentials of its relationship to the habitat. *The American Naturalist*, *107*(954), 213–246. https://doi.org/10.1086/282827

Marchal, A., Schlichting, C. D., Gobin, R., Balandier, P., Millier, F., Muñoz, F., … Sánchez, L. (2019). Deciphering hybrid larch reaction norms using random regression. *G3: Genes, Genomes, Genetics*, *9*(1), 21–32. https://doi.org/10.1534/g3.118.200697

Martin, J. T., Pederson, G. T., Woodhouse, C. A., Cook, E. R., McCabe, G. J., Wise, E. K., … King, J. (2019). 1200 years of Upper Missouri River streamflow reconstructed from tree rings. *Quaternary Science Reviews*, *224*, 105971. https://doi.org/10.1016/j.quascirev.2019.105971

Martin-Benito, D., Kint, V., del Río, M., Muys, B., & Cañellas, I. (2011). Growth responses of West-Mediterranean *Pinus nigra* to climate change are modulated by competition and productivity: Past trends and future perspectives. *Forest Ecology and Management*, *262*(6), 1030–1040. https://doi.org/10.1016/j.foreco.2011.05.038

Martínez-Vilalta, J., López, B. C., Loepfe, L., & Lloret, F. (2012). Stand- and tree-level determinants of the drought response of Scots pine radial growth. *Oecologia*, *168*(3), 877–888. https://doi.org/10.1007/s00442-011-2132-8

Merchant, N., Lyons, E., Goff, S., Vaughn, M., Ware, D., Micklos, D., & Antin, P. (2016). The iPlant collaborative: Cyberinfrastructure for enabling data to discovery for the life sciences. *PLoS Biology*, *14*(1), e1002342. https://doi.org/10.1371/journal.pbio.1002342

Mina, M., Martin-Benito, D., Bugmann, H., & Cailleret, M. (2016). Forward modeling of tree-ring width improves simulation of forest growth responses to drought. *Agricultural and Forest Meteorology*, *221*, 13–33. https://doi.org/10.1016/j.agrformet.2016.02.005

Montwé, D., Isaac-Renton, M., Hamann, A., & Spiecker, H. (2016). Drought tolerance and growth in populations of a wide-ranging tree species indicate climate change risks for the boreal north. *Global Change Biology*, *22*(2), 806–815. https://doi.org/10.1111/gcb.13123

Montwé, D., Spiecker, H., & Hamann, A. (2015). Five decades of growth in a genetic field trial of Douglas-fir reveal trade-offs between productivity and drought tolerance. *Tree Genetics & Genomes*, *11*(2), 29. https://doi.org/10.1007/s11295-015-0854-1

Morrongiello, J. R., & Thresher, R. E. (2015). A statistical framework to explore ontogenetic growth variation among individuals and populations: A marine fish example. *Ecological Monographs*, *85*(1), 93–115. https://doi.org/10.1890/13-2355.1

O'Connor, C. D., Falk, D. A., Lynch, A. M., & Swetnam, T. W. (2014). Fire severity, size, and climate associations diverge from historical precedent along an ecological gradient in the Pinaleño Mountains, Arizona, USA. *Forest Ecology and Management*, *329*, 264–278. https://doi.org/10.1016/j.foreco.2014.06.032

Pan, Y., Birdsey, R. A., Fang, J., Houghton, R., Kauppi, P. E., Kurz, W. A., … Hayes, D. (2011). A large and persistent carbon sink in the world's forests. *Science*, *333*(6045), 988–993. https://doi.org/10.1126/science.1201609

Parent, B., Turc, O., Gibon, Y., Stitt, M., & Tardieu, F. (2010). Modelling temperature-compensated physiological rates, based on the co-ordination of responses to temperature of developmental processes. *Journal of Experimental Botany*, *61*(8), 2057–2069. https://doi.org/10.1093/jxb/erq003

Pederson, G. T., Gray, S. T., Woodhouse, C. A., Betancourt, J. L., Fagre, D. B., Littell, J. S., … Graumlich, L. J. (2011). The unusual nature of recent snowpack declines in the North American Cordillera. *Science*, *333*(6040), 332–335. https://doi.org/10.1126/science.1201570

Peterson, D. W., Peterson, D. L., & Ettl, G. J. (2002). Growth responses of subalpine fir to climatic variability in the Pacific Northwest. *Canadian Journal of Forest Research*, *32*(9), 1503–1517. https://doi.org/10.1139/x02-072

Pickett, S. T. A. (1989). Space-for-time substitution as an alternative to long-term studies. In G. E. Likens (Ed.), *Long-term studies in ecology: Approaches and alternatives* (pp. 110–135). New York, NY: Springer.

R Core Team. (2018). R: A language and environment for statistical computing. R Foundation for Statistical Computing: Retrieved from. https://www.R-project.org/.

Razavi, S., Elshorbagy, A., Wheater, H., & Sauchyn, D. (2015). Toward understanding nonstationarity in climate and hydrology through tree ring proxy records. *Water Resources Research*, *51*(3), 1813–1830. https://doi.org/10.1002/2014WR015696

Redmond, M. D., Kelsey, K. C., Urza, A. K., & Barger, N. N. (2017). Interacting effects of climate and landscape physiography on piñon pine growth using an individual-based approach. *Ecosphere*, *8*(3), e01681. https://doi.org/10.1002/ecs2.1681

Restaino, C. M., Peterson, D. L., & Littell, J. (2016). Increased water deficit decreases Douglas fir growth throughout western US forests. *Proceedings of the National Academy of Sciences of the United States of America*, *113*(34), 9557–9562. https://doi.org/10.1073/pnas.1602384113

Rollinson, C. R., Liu, Y., Raiho, A., Moore, D. J. P., McLachlan, J., Bishop, D. A., … Dietze, M. C. (2017). Emergent climate and CO_2 sensitivities of net primary productivity in ecosystem models do not agree with empirical data in temperate forests of eastern North America. *Global Change Biology*, *23*(7), 2755–2767. https://doi.org/10.1111/gcb.13626

Ryerson, D. E., Swetnam, T. W., & Lynch, A. M. (2003). A tree-ring reconstruction of western spruce budworm outbreaks in the San Juan Mountains, Colorado, U.S.A. *Canadian Journal of Forest Research*, *33*(6), 1010–1028. https://doi.org/10.1139/x03-026

Schlichting, C. D. (1986). The evolution of phenotypic plasticity in plants. *Annual Review of Ecological Systems*, *17*, 667–693. https://doi.org/10.1146/annurev.es.17.110186.003315

Schurgers, G., Ahlström, A., Arneth, A., Pugh, T. A. M., & Smith, B. (2018). Climate sensitivity controls uncertainty in future terrestrial carbon sink. *Geophysical Research Letters*, *45*(9), 4329–4336. https://doi.org/10.1029/2018GL077528

Sitch, S., Friedlingstein, P., Gruber, N., Jones, S. D., Murray-Tortarolo, G., Ahlström, A., … Myneni, R. (2015). Recent trends and drivers of regional sources and sinks of carbon dioxide. *Biogeosciences*, *12*(3), 653–679. https://doi.org/10.5194/bg-12-653-2015

Stewart, C. A., Turner, G., Vaughn, M., Gaffney, N. I., Cockerill, T. M., Foster, I., … Tuecke, S.. (2015). Jetstream: a self-provisioned, scalable science and engineering cloud environment. *Proceedings of the 2015 XSEDE Conference on Scientific Advancements Enabled by Enhanced Cyberinfrastructure – XSEDE*, *15*, 1–8. https://doi.org/10.1145/2792745.2792774

Swetnam, T., & Lynch, A. (1989). A tree-ring reconstruction of western spruce budworm history in the southern rocky mountains. *Forest Science*, *35*(4), 962–986.

Taeger, S., Zang, C., Liesebach, M., Schneck, V., & Menzel, A. (2013). Impact of climate and drought events on the growth of Scots pine (*Pinus sylvestris* L.) provenances. *Forest Ecology and Management*, *307*, 30–42. https://doi.org/10.1016/j.foreco.2013.06.053

Towns, J., Cockerill, T., Dahan, M., Foster, I., Gaither, K., Grimshaw, A., … Wilkins-Diehr, N. (2014). XSEDE: Accelerating scientific discovery. *Computing in Science Engineering*, *16*(5), 62–74. https://doi.org/10.1109/MCSE.2014.80

Urban, O., Košvancová, M., Marek, M. V., & Lichtenthaler, H. K. (2007). Induction of photosynthesis and importance of limitations during the induction phase in sun and shade leaves of five ecologically contrasting tree species from the temperate zone. *Tree Physiology*, *27*(8), 1207–1215. https://doi.org/10.1093/treephys/27.8.1207

Via, S., & Lande, R. (1985). Genotype-environment interaction and the evolution of phenotypic plasticity. *Evolution*, *39*(3), 505–522. https://doi.org/10.1111/j.1558-5646.1985.tb00391.x

Vicente-Serrano, S. M., Beguería, S., & López-Moreno, J. I. (2010). A multiscalar drought index sensitive to global warming: The standardized precipitation evapotranspiration index. *Journal of Climate*, *23*(7), 1696–1718. https://doi.org/10.1175/2009JCLI2909.1

Wang, T., Hamann, A., Spittlehouse, D., & Carroll, C. (2016). Locally downscaled and spatially customizable climate data for historical and future periods for North America. *PLoS ONE*, *11*(6), e0156720. https://doi.org/10.1371/journal.pone.0156720

Watson, E., & Luckman, B. H. (2002). The dendroclimatic signal in Douglas-fir and ponderosa pine tree-ring chronologies from the southern Canadian Cordillera. *Canadian Journal of Forest Research*, *32*(10), 1858–1874. https://doi.org/10.1139/x02-096

Wehrens, P., & Buydens, L. M. C. (2007). Self- and super-organizing maps in R: The kohonen package. *Journal of Statistical Software*, *21*(5), 1–19. https://doi.org/10.18637/jss.v021.i05.

Weiskittel, A. R., Crookston, N. L., & Radtke, P. J. (2011). Linking climate, gross primary productivity, and site index across forests of the western United States. *Canadian Journal of Forest Research*, *41*(8), 1710–1721. https://doi.org/10.1139/x11-086

Williams, A. P., Allen, C. D., Macalady, A. K., Griffin, D., Woodhouse, C. A., Meko, D. M., … McDowell, N. G. (2013). Temperature as a potent driver of regional forest drought stress and tree mortality. *Nature Climate Change*, *3*(3), 292–297. https://doi.org/10.1038/nclimate1693

Wilmking, M., van der Maaten-Theunissen, M., van der Maaten, E., Scharnweber, T., Buras, A., Biermann, C., … Trouillier, M. (2020). Global assessment of relationships between climate and tree growth. *Global Change Biology*, *26*, 3212–3220. https://doi.org/10.1111/gcb.15057

Wilson, R., Anchukaitis, K., Briffa, K. R., Büntgen, U., Cook, E., D'Arrigo, R., … Zorita, E. (2016). Last millennium northern hemisphere summer temperatures from tree rings: Part I: The long term context. *Quaternary Science Reviews*, *134*, 1–18. https://doi.org/10.1016/j.quascirev.2015.12.005

Zhang, Q.-B., & Hebda, R. J. (2004). Variation in radial growth patterns of *Pseudotsuga menziesii* on the central coast of British Columbia, Canada. *Canadian Journal of Forest Research*, *34*(9), 1946–1954. https://doi.org/10.1139/x04-078

Zuidema, P. A., Poulter, B., & Frank, D. C. (2018). A wood biology agenda to support global vegetation modelling. *Trends in Plant Science*, *23*(11), 1006–1015. https://doi.org/10.1016/j.tplants.2018.08.003

SUPPORTING INFORMATION

Additional supporting information may be found online in the Supporting Information section.

How to cite this article: Klesse S, DeRose RJ, Babst F, et al. Continental-scale tree-ring-based projection of Douglas-fir growth: Testing the limits of space-for-time substitution. *Glob Change Biol*. 2020;00:1–18. https://doi.org/10.1111/gcb.15170